HHS Public Access

Author manuscript

J Comp Neurol. Author manuscript; available in PMC 2022 March 01.

Published in final edited form as:

J Comp Neurol. 2021 March ; 529(4): 885–904. doi:10.1002/cne.24986.

Distribution and overlap of entorhinal, premotor, and amygdalar connections in the monkey anterior cingulate cortex

Samantha M. Calderazzo[1,2], **Silas E. Busch**[1,3], **Tara L. Moore**[1,2], **Douglas L. Rosene**[1,2], **Maria Medalla**[1,2]

[1]Department of Anatomy & Neurobiology, Boston University School of Medicine, Boston, Massachusetts

[2]Center for Systems Neuroscience, Boston University, Boston, Massachusetts

[3]Department of Neurobiology, University of Chicago, Chicago, Illinois

Abstract

The anterior cingulate cortex (ACC) is important for decision-making as it integrates motor plans with affective and contextual limbic information. Disruptions in these networks have been observed in depression, bipolar disorder, and post-traumatic stress disorder. Yet, overlap of limbic and motor connections within subdivisions of the ACC is not well understood. Hence, we administered a combination of retrograde and anterograde tracers into structures important for contextual memories (entorhinal cortex), affective processing (amygdala), and motor planning (dorsal premotor cortex) to assess overlap of labeled projection neurons from (outputs) and axon terminals to (inputs) the ACC of adult rhesus monkeys (*Macaca mulatta*). Our data show that entorhinal and dorsal premotor cortical (dPMC) connections are segregated across ventral (A25, A24a) and dorsal (A24b,c) subregions of the ACC, while amygdalar connections are more evenly distributed across subregions. Among all areas, the rostral ACC (A32) had the lowest relative density of connections with all three regions. In the ventral ACC, entorhinal and amygdalar connections strongly overlap across all layers, especially in A25. In the dorsal ACC, outputs to dPMC and the amygdala strongly overlap in deep layers. However, dPMC input to the dorsal ACC was densest in deep layers, while amygdalar inputs predominantly localized in upper layers. These connection patterns are consistent with diverse roles of the dorsal ACC in motor evaluation and the ventral ACC in affective and contextual memory. Further, distinct laminar circuits suggest unique

Correspondence Maria Medalla, 72 East Concord St L1001, Boston, MA 02118. mmedalla@bu.edu.

AUTHOR CONTRIBUTIONS

SM Calderazzo, SE Busch, TL Moore, DL Rosene, and M Medalla performed experiments; SM Calderazzo and SE Busch performed data gathering and analyses; SM Calderazzo and M Medalla performed statistical analyses and wrote the first draft of the manuscript. SM Calderazzo, SE Busch, TL Moore, DL Rosene, and M Medalla edited the manuscript and approved the final version.

CONFLICT OF INTEREST

The authors declare no conflict of interest.

ETHICAL STATEMENT

All experimental procedures were conducted in accordance with the U.S. National Research Council's “Guide for the Care and Use of Laboratory Animals,” the U.S. Public Health Service's “Policy on Humane Care and Use of Laboratory Animals,” and “Guide for the Care and Use of Laboratory Animals.”

PEER REVIEW

The peer review history for this article is available at https://publons.com/publon/10.1002/cne.24986.

interactions within specific ACC compartments that are likely important for the temporal integration of motor and limbic information during flexible goal-directed behavior.

Keywords

dorsal premotor cortex; medial prefrontal cortex; medial temporal; non-human primate; RRID: AB_2340397; RRID: SCR_002526; RRID:AB_221558; RRID:AB_221561; RRID:AB_2313606; RRID:AB_2336382; RRID:AB_2336819; RRID:AB_2536192; RRID:AB_2536196; RRID:SCR_000432; RRID:SCR_001622; RRID:SCR_002465; tract-tracing

1 | INTRODUCTION

The anterior cingulate cortex (ACC) is part of the executive frontal network that is critical for cognitive-emotional-motor integration during decision-making (Barbas, 1995; Barbas & Zikopoulos, 2007; Bush, Luu, & Posner, 2000; Etkin, Egner, & Kalisch, 2011; Kennerley & Walton, 2011; Paus, 2001; Pessoa, 2010; Stevens, Hurley, & Taber, 2011). For goal-directed behavior, contextual and affective information from medial temporal memory circuits need to reach motor planning centers. Conversely, motor plans and decisions are encoded into memory via medial temporal circuits to guide future action. However, the medial temporal and motor cortical system have very sparse direct connections, and communicate predominantly via indirect cortical and subcortical routes (e.g., Dum & Strick, 2002; Insausti, Amaral, & Cowan, 1987; Saunders, Rosene, & Van Hoesen, 1988). One important cortical route is through the ACC, which has extensive connections with entorhinal and parahippocampal cortices of the medial temporal lobe (Anderson, Bunce, & Barbas, 2016; Barbas & Blatt, 1995; Barbas & De Olmos, 1990; Blatt, Pandya, & Rosene, 2003; Blatt & Rosene, 1988; Bunce & Barbas, 2011; Insausti et al., 1987; Insausti & Amaral, 2008; Joyce & Barbas, 2018; Kondo, Saleem, & Price, 2005; Lavenex, Suzuki, & Amaral, 2002; Mohedano-Moriano et al., 2007; Munoz & Insausti, 2005; Pandya, Van Hoesen, & Mesulam, 1981; Rempel-Clower & Barbas, 2000; Rosene & Van Hoesen, 1977; Saleem, Kondo, & Price, 2008; Suzuki & Amaral, 2004; Zikopoulos, Hoistad, John, & Barbas, 2017), as well as, premotor cortices (Barbas & Pandya, 1987; Bates & Goldman-Rakic, 1993; Carmichael & Price, 1995; Dum & Strick, 1992, 2002; Luppino, Rozzi, Calzavara, & Matelli, 2003; Morecraft et al., 2012). Additionally, the ACC has strong connections with the amygdala, a medial temporal structure important for regulating emotional arousal and motivational drive (Barbas & De Olmos, 1990; Barbas, Saha, Rempel-Clower, & Ghashghaei, 2003; Ghashghaei & Barbas, 2002; Kim et al., 2018; Phelps, 2004; Sharma, Kelly, Pfeifer, & Fudge, 2019; Vogt, 2005). How these medial temporal limbic systems interact with the motor planning system, and how they converge and diverge across distinct subdivisions and cortical layers of the ACC, is not well-understood.

The entorhinal cortex is a convergence point for the hippocampal formation and multimodal sensory association areas, and has a critical role in episodic or contextual learning and memory (Eichenbaum & Lipton, 2008; Hinman, Dannenberg, Alexander, & Hasselmo, 2018; Killian, Jutras, & Buffalo, 2012; Sasaki, Leutgeb, & Leutgeb, 2015). Through direct connections with rhinal and parahippocampal cortices, the ACC is thought to be important for gating information flow to and from the hippocampus (e.g., Bunce & Barbas, 2011;

Joyce & Barbas, 2018; Paz, Bauer, & Pare, 2007) (review: Barbas, Bunce, & Medalla, 2012). Thus, the ACC is in a position to access and control emotional arousal and contextual memory systems via medial temporal connections, and planned action via premotor connections, consistent with its role in the affective aspects of motor responses and performance evaluation (e.g., Botvinick, Cohen, & Carter, 2004; Hayden & Platt, 2010; Ito, Stuphorn, Brown, & Schall, 2003; Monosov & Hikosaka, 2012; Rudebeck et al., 2014). For example, activity in the ACC is related to motor inhibition of irrelevant responses (Ito et al., 2003; Johnston, Levin, Koval, & Everling, 2007), error monitoring (Niki & Watanabe, 1979; Shen et al., 2015), as well as perception of negative affect (Amemori & Graybiel, 2012; Ichikawa et al., 2011; Onoda et al., 2009) or noxious stimuli (Vogt, 2005). Disruption of these ACC pathways can lead to misattribution of memories and motivational context for goal-directed action, as seen in depression, bipolar disorder, and post-traumatic stress disorder (review: Drevets, Savitz, & Trimble, 2008; Rauch, Shin, & Phelps, 2006; Workman et al., 2016).

Previous work has shown the existence and general topography of these medial temporal and premotor ACC connections. However, the quantitative distribution of these pathways and precisely how they interface within distinct cytoarchitectonic areas (BA 24a, 24b, 24c, 25, and 32) and layers of the ACC are not well-understood. Furthermore, the specific quantitative laminar input–output organization of EC pathways within the ACC is not known. In this study, we injected anterograde and retrograde tracers into the dorsal premotor cortex (dPMC), amygdala (AMY), and entorhinal cortex (EC) of rhesus macaques in order to quantitatively assess inputs and outputs of these structures within distinct subdivisions of the ACC (A24a, A24b, A24c, A25, and A32). We specifically examined laminar patterns of connectivity and overlap to highlight bidirectional organization and topography of these three systems. Understading these pathway connections will shed light on how multimodal memory and motivational information may be integrated and processed in the ACC to guide goal-directed behavior.

2 | METHODS

2.1 | Experimental model and subject details

A total of five adult rhesus monkeys (*Macaca mulatta*; 6 ± 0.3 years old; range = 5–7 years old; three males, two females) received a combination of injections of the dextran amine bidirectional tracers fluororuby (FR), fluoroemerald (FE), and Cascade Blue (CBL) in the dPMC, AMY, and EC in the R hemisphere (Figures 1-4 and Table 1). Monkeys were obtained from national primate research facilities or private vendors and all had known birth dates and complete health records. Monkeys were housed in the Animal Science Center (ASC) at Boston University School of Medicine (BUSM) and kept under a 12-hr light/dark cycle. ASC is fully accredited by the Association for Assessment and Accreditation of Laboratory Animal Care. All animal research was conducted in strict accordance with the guidelines established by the NIH *Guide for the Care and Use of Laboratory Animals* and the *U.S. Public Health Service Policy on Humane Care and Use of Laboratory Animals* and was approved by the Boston University Institutional Animal Care and Use Committee.

2.2 | Surgical procedures and injection of neural tracers

Injections of neural tracers were made using magnetic resonance imaging (MRI) and surgical procedures described previously (Medalla & Barbas, 2009; Medalla, Lera, Feinberg, & Barbas, 2007). Injection sites were based on stereotaxic coordinates calculated from MRI scans taken prior to surgery, using the midline and betadine-filled ear bar tips as reference points. For MRI procedures, monkeys were sedated with ketamine hydrochloride and deeply anesthetized with propofol (to effect) and scanned with the head stabilized in an MRI compatible stereotaxic apparatus. For survival surgery, monkeys were deeply anesthetized with isoflurane (1–3%, to effect) and positioned in the same MRI compatible stereotaxic apparatus (Kopf 1530, David Kopf Instruments; Tujunga, CA), and a small opening was made in the skull and dura, followed by tracer injections in the regions of interest (Figure 1a-e and Table 1). In each hemisphere, a combination of regions of interest were each injected with fluoroemerald (FE, dextran fluorescein cat#s D1820 & D3305), fluororuby (FR, dextran tetramethylrhodamine, cat#s D1817 & D3308), or Cascade Blue (CBL, cat#s D7132 & D1976 Thermo Fisher) dextran amines using a micro-syringe (5 or 10 μl; Hamilton, Reno, NV) mounted on a microdrive. Both 3- and 10-kDA isoforms of dextran amines were used to ensure enhanced bidirectional retrograde and anterograde transport (Reiner et al., 2000; Veenman, Reiner, & Honig, 1992). For each injection, the dye was diluted to 10 mg/ml in distilled water and delivered in 2–3 μl volumes at each injection site. Two to three dPMC injections were delivered (spaced 0.5 mm apart) at a depth of 1.5 mm below the pial surface of the rostral dorsal PMC. One injection each was delivered into the AMY basolateral complex or the anterior EC. For each injection, the needle was left in situ for 10 min to allow for diffusion and prevent upward suction of the dye upon retraction of the needle. Tracer injection site locations and volumes are summarized in Table 1.

2.3 | Perfusion and tissue harvesting

After a survival period of 21 days, harvesting of the brain and whole brain fixation was performed using our standard two-stage Krebs-paraformaldehyde perfusion method as described (Amatrudo et al., 2012). The animals were deeply anesthetized with sodium pentobarbital (to effect, 25 mg/kg, i.v.), then perfused through the ascending aorta first with ice-cold Krebs–Henseleit buffer (concentrations, in mM: 6.4 Na_2HPO_4, 1.4 Na_2PO_4, 137 NaCl, 2.7 KCl, 5 Glucose, 0.3 $CaCl_2$, 1 $MgCl_2$; pH 7.4, Sigma-Aldrich, St. Louis, MO), during which fresh tissue biopsies of the left hemisphere were taken for other studies. Promptly after fresh tissue collection, perfusate was switched to freshly depolymerized 4% paraformaldehyde (EM grade; Ladd Research Industries, Williston, VT) in 0.1 M phosphate buffer (PB) (pH 7.4, at 37°C) to fix the remainder of the left hemisphere and the intact right hemisphere for whole brain tracer mapping. The brain was blocked *in situ* in the coronal plane then removed from the skull, cryoprotected in graded solutions of glycerol (10–20%) in 0.1 M PB with 2% DMSO, followed by flash freezing in −75°C isopentane (Rosene, Roy, & Davis, 1986). It was then stored at −80°C until cut on a freezing microtome in the coronal plane at 60 μm. Tissue sections were stored in anti-freeze solution (30% ethylene glycol, 30% glycerol, in 0.05 M PB, pH 7.4 with 0.05% azide) at −20°C until used.

2.4 | Immunohistochemistry of thin sections for brightfield and confocal microscopy

For stereological counting of labeled neurons and boutons, one series (representing 1 in 40 sections) of 60-μm coronal sections from the intact right hemisphere was processed for immunohistochemistry to photoconvert fluorescent tracers to brightfield labeling as described (Medalla et al., 2007; Medalla & Barbas, 2009). Free-floating sections (at 4°C) were processed, pre-blocked and incubated overnight in antibodies against FE (1:800 mouse monoclonal RRID:AB_221561 or goat polyclonal RRID:AB_221558, Thermo Fisher), FR (1:800, rabbit polyclonal, RRID:AB_2536196, Thermo Fisher), or CBL (1:800, rabbit polyclonal, RRID:AB_2536192, Thermo Fisher) diluted in 0.1 M PB, 1% NDS, 0.2% BSAc, 0.1% Triton-X. Sections were then incubated for 2 hr (at 4°C) in biotinylated goat anti-rabbit (RRID:AB_2313606, Vector Laboratories) or donkey anti-goat secondary IgG (RRID: AB_2340397, Jackson Immunoresearch; 1:200, for 2 hr), followed by 1 hr at room temperature in avidin–biotin with horseradish peroxidase (AB-HRP) solution (Vectastain PK-6100 ABC Elite kit, RRID:AB_2336819, Vector). Sections were processed to visualize label using the peroxidase-catalyzed polymerization of diaminobenzidine (DAB, for 2–3 min; DAB kit SK-4100, RRID:AB_2336382; Vector). After processing, sections were mounted on gelatin-coated slides, counterstained with thionin (Sigma Aldrich) to delineate cytoarchitectonic areas and cortical layers, dehydrated in alcohol, and coverslipped with Entellan (Sigma Aldrich).

To confirm and visualize pathway overlap, we used dual-immunofluorescence labeling to amplify tracer-labeled signal in axons and projection neuron dendrites. Sections were co-incubated overnight (4°C) in primary antibodies against the tracer fluorophores FE (1:800, mouse monoclonal; or goat polyclonal), FR (1:800, rabbit polyclonal), or CBL (1:800, rabbit polyclonal). Sections were then incubated overnight (4°C) in color-matched Alexa-conjugated secondary antibodies raised in donkey (1:200). In order to use two rabbit antibodies (FR and CBL tracers), labelling was performed sequentially and with a customized rabbit-on-rabbit blocking solution containing unconjugated goat-anti-rabbit FAB fragments (Jackson Immunoresearch), as modified from (Medalla & Barbas, 2009). Sections were incubated in the first rabbit primary antibody against CBL (1:800, rabbit polyclonal), then in biotinylated secondary goat anti-rabbit FAB IgG (1:200, for 3 hr at room temperature), followed by Strepatividin-Alexa647 conjugate (1:200, overnight, 4°C). Sections were rinsed and then incubated in unconjugated goat-anti-rabbit FAB fragments (1:200, 2 hr in room temperature, Jackson Immunoresearch) to block any free rabbit IgGs and minimize cross reaction with the second antibody. Sections were then subsequently incubated in the second rabbit primary antibody against FR (1:800, rabbit polyclonal), followed by a secondary donkey anti-mouse IgG conjugated to Alexa 546. To improve antibody penetration, two 10-min microwave sessions at 150 W were run for each incubation step, as described (Medalla, Gilman, Wang, & Luebke, 2017). Sections were mounted on glass slides and cover-slipped with Prolong anti-fade medium (Thermo Fisher).

2.5 | Mapping of retrograde-labeled neurons and anterograde-labeled boutons

2.5.1 | Cytoarchitectonic boundaries and areal nomenclature—Coronal sections Nissl counterstained with thionin were used to quantify label in distinct areas of the ACC, which were delineated based on the architectonic map of Barbas and Pandya (1989) and

brodmann's areas (A24a,b,c, A25, A32). Specifically, we examined architectonic areas within the ventral ACC (vACC: A25, A24a), dorsal ACC (dACC: A24b,c), and rostral ACC (rACC: A32) (Figure 1f). A32 is the most rostral area of the ACC, located rostral to the genu of the corpus callosum (pregenually), which is the gyrus on the medial wall extending from the ventral bank of the cingulate sulcus to the dorsal bank of the rostral sulcus. A25 is posterior to A32, ventral to the genu and rostrum of the corpus callosum, and part of the ventral ACC. A24 occupies the ventral bank of the cingulate sulcus, posterior to A32, extends down the gyrus to the corpus callosum, and is divided into three subareas. The most dorsal ACC subregion, A24c, is burried within the ventral bank of the cingulate sulcus, and is adjacent to A24b, which occupies the lip of the gyrus. A24a is the gyral cortex directly adjacent to the corpus callosum, which has a dorsal and ventral component. Cytoarchitectonically, A32 is distinguished from A25 by the prominent horizontal banding of the cell-dense L5-6. Compared to A32, A25 has a less-organized layers 5–6 and appears to have a greater cell density. At the caudal dACC level, A24c has the most well-delineated cortical layers, followed by A24b, which contains significant laminar stretching in the gyrus, and then A24a, which is the most dysgranular and has the least distinct layer 4. Adjacent to A24a, right against the corpus callosum, is the medial periallocortex (MPall), which was counted within the A24a region of interest (ROI). A24a is distinguished from A24b dorsally and from A25 ventrally by its disorganized and poorly-defined layers.

2.5.2 | Stereological counting methods—For each ROI, three to four evenly-spaced (1 in every 40) coronal sections were used per case, excluding the absolute rostral or caudal edges of the ROI. Using a brightfield microscope (Nikon E600) coupled to a commercial stereological counting software computer system (Stereoinvestigator, RRID: SCR_002526; Microbrightfield, Williston, VT), contours of distinct cortical layers per area were traced. Counting was performed using systematic unbiased sampling with an optical dissector restricted to the central fraction of the post-processing tissue thickness (10 μm). Guard zones (≥2 μm) were placed in the top and bottom of each section to avoid error as a result of uneven tissue sectioning. The counting frame/dissector area (neurons = 100 × 100 μm; boutons = 50 × 50 μm) and sampling grid spacing area were set to employ an area sampling fraction of 50% for boutons and 50–100% for neurons, which yielded coefficient of errors of 5% or less (for reviews see Schmitz & Hof, 2005; West, Slomianka, & Gundersen, 1991). The total volume (mm^3) of each ROI was estimated with the Cavalieri method in order to calculate density. Anterograde-labeled axonal terminals were manually identified and stereologically counted using a 60 × 1.3 NA oil objective, within the following ROIs: L1, L2–3, L4, and L5–6. By focusing up and down the z-extent of the section, labeled axon terminals were identified based on 3D shape and spatial arrangement as boutons or varicosities observed along an axon's longitudinal axis (Figure 2a). The identification of boutons confirmed to be located along visible axons ensures that transversely cut axons are not counted. However, due to the diffraction limits of light microscopy, we are likely missing a subset of thin axons and terminals smaller than ~250 nm in diameter. Labeled neurons were manually counted within upper L2-3 and deep L5-6 using a 20× objective (Figure 2b). The relative densities of inputs to (tracer-labeled axon terminals) and outputs from (tracer-labeled projection neurons) these laminar ROIs were estimated in distinct ACC areas A32, A25, A24a, A24b, and A24c.

To account for the variability of labeling due to differences in the volume of the injections, we normalized data by expressing it as relative regional or laminar density, as described in previous quantitative anatomical studies (e.g., Fudge, deCampo, & Becoats, 2012; Ghashghaei & Barbas, 2002; Hilgetag, Medalla, Beul, & Barbas, 2016; Insausti et al., 1987; Medalla et al., 2007; Mohedano-Moriano et al., 2007). Specifically for each injection case, we first calculated the absolute density (D) in each ACC area (regional) or cortical layer (laminar) by dividing the estimated number (N) of elements (boutons or neurons) by the estimated volume (V) of each ROI ($D_{(region)abs} = N_{(region)}/ V_{(region)}$; $D_{(layer)abs} = N_{(layer)}/ V_{(layer)}$). We then calculated relative densities in a given ROI by normalizing the absolute density in each area ($D_{(region)abs}$) or layer ($D_{(layer)abs}$) with the summation of absolute densities from all ACC areas examined in the injection case ($\Sigma D_{(ACC)abs}$; for each case, the relative regional density: $D_{(region)rel} = D_{(region)abs}/\Sigma D_{(ACC)abs}$; relative laminar density $D_{(layer)rel} = D_{(layer)abs}/\Sigma(D_{(ACC)abs})$]. This normalization was done for each injection case, and the means of these normalized values were used for statistical comparison.

2.5.3 | Confocal microscopy imaging—To visualize labeled fibers and neurons from two pathways together in one field, two-channel confocal image stacks were acquired (Zeiss 710; 63× 1.3 NA, oil immersion; 0.07 × 0.07 × 0.3 μm voxel). Based on the density results from stereological analyses, we subsampled and imaged the entire *z*-extent of the 60-μm section of 2–3 fields in each cortical layer throughout a cortical column (pia to white matter) from ACC areas with dense overlap of the two labeled connections. Image stacks were then deconvolved using AutoQuant (RRID:SCR_002465; Media Cybernetics, Bethesda, MD).

2.6 | Statistical analyses

Statistical analyses were conducted in RStudio (R3.25, RStduio, Boston, MA; RRID:SCR_000432) or MATLAB (R2018, Mathworks, Natick, MA; RRID:SCR_001622). In order to assess regional differences, multi- and single-factorial ANOVAs of normalized regional density of neurons or boutons from each injection site were compared across ROIs in RStudio, including sex as a variable. ANOVAS showed no significant interactions with sex. In order to assess laminar interactions and input/output analyses, variables were compared using generalized linear equations and multifactorial ANOVAs in MATLAB, including sex as a variable. Multiple regression analyses showed no significant effects of sex in the variables measured. Relationships between variables were determined using linear and non-linear regression analyses conducted in MATLAB. Significance was set at $\alpha \leq 0.05$ for all statistical tests. Non-metric multidimensional scaling (NMDS) was performed to analyze similarities among individual ACC areas in each case, based on 12 outcome measures of regional and laminar connections (AMY, PMC and EC anterograde and retrograde relative regional densities, % upper layer neurons and % deep layer axon terminals normalized for each area), as described previously (Dombrowski, Hilgetag, & Barbas, 2001; Gilman, Medalla, & Luebke, 2017; Hilgetag, Burns, O'Neill, Scannell, & Young, 2000; Hsu, Luebke, & Medalla, 2017; Young et al., 1995). Since not all cases had all three injections, means for each variable were used to substitute for missing values. For each variable, *z*-scores were obtained, and pair-wise comparisons were used to calculate a distance matrix based on squared Euclidean distances. The multidimensional distance matrix was then reduced to two dimensions via NMDS, and the resulting values of each area per case was plotted, with the

distances between data points representing the relative similarities based on the set of variables.

3 | RESULTS

3.1 | Injection sites

Injections in the EC (cases PIJ, PIM, PIN) were restricted to the anterior third of the rostro-caudal extent of the EC (Figure 1a,c and Table 1). Injection sites in the dPMC spanned ~2 mm along the rostro-caudal axis, and were restricted to the rostral half of the dorsomedial PMC—the supplementary motor area 6DR or area F7 and F6 (Figure 1a,b) (Barbas & Pandya, 1987; Morecraft et al., 2012; Schall, Morel, & Kaas, 1993; Van Hoesen & Vogt, 1993). Injections in the AMY were localized to the basolateral complex with slight variation in the precise nuclei involved (Barbas & De Olmos, 1990; Fudge et al., 2012; Ghashghaei & Barbas, 2002; Iwai & Yukie, 1987; Pitkanen & Amaral, 1994) (Figure 1a,d,e and Table 1). In case PIK, the core of the injection site was restricted to the middle of the basolateral nucleus, while in case PIL, the core was located at the medial border of the lateral nucleus (Figure 1d,e). In cases PIM, PIN, and PIJ, the core of the injection site was located more anteriorly within the basomedial nucleus in PIM and within the cortical nucleus in case PIJ (not shown) and PIN (Figure 1d,e).

3.2 | The EC predominantly connects with the ventral ACC areas 25 and 24a

We estimated the relative density of anterograde-labeled axon terminals from the EC (inputs) and retrograde-labeled projection neurons to the EC (outputs) across ACC A32, A25, and A24a, 24b, and 24c. (Figure 2c,d and 3). We found that labeled terminals from the EC were consistently most dense in the vACC A25 and A24a ($n = 3$ cases for each area; ANOVA with Tukey post-hoc test ($F(4,10) = 46.58$, $p < 1.0e\text{-}5$; Figures 2c and 3a). The relative density of labeled terminals in A24a was significantly higher than in A24b, A24c, and A32 ($p < .05$). A25 had the greatest density of terminations compared to all other regions ($p < .05$). The laminar termination pattern of EC inputs (Figure 3a) was distinct across ACC areas. Anterograde-labeled axon terminals in the upper versus deep layers were equally distributed in A25, A24a and A32, but exhibited a bias for the upper layers in A24b and A24c.

Similar to anterograde label, the density of retrograde-labeled projection neurons from ACC to EC showed the same regional distribution; projection neurons were consistently most dense in A25 and A24a (n = 3 cases for each area; ANOVA with Tukey Post-hoc test, ($F(4,20) = 21.26$, $p < 1.0e\text{-}6$; Figures 2d and 3b). A25 had the greatest relative density of projection neurons compared to all other regions ($p < .005$). Retrograde-labeled projection neurons to EC were evenly distributed across upper and deep layers of ACC areas, except for A25, where projection neurons mainly emanated from the deep layers (Figure 3b).

3.3 | The dPMC predominantly connects with the dorsal ACC areas 24b and c

In contrast to the EC connections, we found that axon terminations from and projection neurons to the dPMC were densest in dACC areas (Figure 4). The relative density of anterograde-labeled axon terminals from the dPMC to the ACC was consistently greater in

the dACC A24b and A24c (n = 3 cases for each area; main effect ANOVA (F(4,10) = 19.54, p < .01; Figure 4a). Pairwise comparisons revealed that, the relative density of dPMC axon terminals in A24c was significantly greater than in A24a, A24b, and A32 (Tukey post-hoc, p < .05), and the density in A24b was significantly greater than in A32 (p < .05). Interestingly, the laminar distribution of dPMC axon terminals (Figure 4a) was distinct across ACC areas, in patterns that were somewhat opposite the EC axon terminals (Figure 3). A25, A24a, and A32 exhibited relatively greater density of terminals in the deep layers, while A24b and A24c exhibited equal proportions of labeled terminals in upper and deep layers.

Similarly, the relative density of retrograde-labeled projection neurons from the ACC to the PMC were also consistently most dense in A24b and A24c (n = 3 cases for each area; main effect ANOVA (F(4,10) = 7.171, p < .001; Figure 4b). A24c had significantly greater relative density of projection neurons to the dPMC compared to A24a, A25, and A32 (Tukey post-hoc, p < .05), and A24b had a significantly greater relative density of projection neurons to the dPMC compared to A32 (Tukey post-hoc, p < .05). These retrograde-labeled projection neurons to the dPMC emanated mainly from the deep layers of the ACC, with a relatively higher laminar density of labeled neurons arising from L5-6 in areas 24b and 24c (Figure 4b,c).

3.4 | The AMY predominantly connects with both dorsal and ventral ACC areas

Compared to the EC and dPMC, AMY connections are more evenly distributed across subdivisions of the ACC (Figure 5). Specifically, the relative density of anterograde-labeled axon terminals from the AMY to the ACC were equally strong in A25 and all subdivisions of A24 (n = 3 cases for each area; main effect ANOVA (F(4,10) = 6.009, p < 0.01; Figure 5a). A32 had significantly lower density of AMY terminations compared to all other regions (Tukey post-hoc, p < .05). Interestingly, the laminar pattern of AMY terminations was similar to the EC, with labeled axon terminals from the AMY equally distributed in the upper versus deep layers of A25, A24a, and A32, and a bias for the upper layers in A24b and A24c (Figure 5a).

Similar to the axonal termination patterns, the relative density of retrograde-labeled projection neurons from the ACC to the AMY were equally distributed across A25 and subdivisions of A24 (n = 3 cases for each area; ANOVA with Tukey post-hoc test, (F(4,10) = 1.861, p = 0.157; Figure 5b. While the absolute density of ACC projection neurons were substantial in all ACC areas, AMY projection neurons from A32 showed the lowest relative density among the ACC areas examined. Although it should be noted that the two cases with more centrally located AMY injections had A32 relative densities about 10 times lower than the subject with a more anteriorly located AMY injection. The laminar origin of projection neurons to the AMY also differed across ACC areas. In A25, A24c, and A32, projection neurons to the AMY arose predominantly from the deep layers. However, in A24a and A24b, laminar origin of projection neurons to the AMY were more evenly distributed across upper and deep layers (Figure 5b,c).

3.5 | Distinct laminar distribution and dorso-ventral shift of EC, AMY, and dPMC connections in ACC

We then examined how the relative laminar distributions of ACC connections to EC, AMY, and dPMC vary within each region of the ACC. We plotted the density of anterograde-labeled axon terminals (inputs) in layers 1, 2–3, 4, and 5–6 of the ACC, normalized to the total summed density of labeled terminations from each injection site and ACC area, and compared their strength in each layer and area (Figure 6a-e). Overall, we found a dorsal to ventral shift from dPMC dominated inputs to EC dominated inputs across all layers.

In the dACC A24c, inputs from all three pathways were found across layers, with a significantly higher relative density of dPMC inputs compared to AMY and EC, especially in the deep layers, while the EC had the lowest density of all pathways (Figure 6a; MANOVA; $F(2,11) = 96.64$, $p < 1.0e\text{-}4$; Tukey's post-hoc, dPMC vs. AMY $p < 0.001$; dPMC vs. EC $p < .001$; AMY vs. EC $p < .01$). In A24b, dPMC inputs were evenly distributed across layers, and both dPMC and AMY inputs predominated over EC inputs ($F(2,11) = 14.04$, $p < .01$; Tukey's post-hoc, EC vs. dPMC $p < .05$; EC vs. AMY $p < .05$), especially in L4 and 5–6. In addition, AMY inputs exhibited a significant peak in density in L2–3 (Figure 6b). In A24a, AMY and EC inputs begin to dominate ($F[2,11] = 10.34$, $P < 0.05$; Tukey's post-hoc, AMY vs. dPMC $p < .05$; EC vs. dPMC $p < .05$) but all pathways show similar laminar patterns, with a peak in density of axon terminals from all pathways in layer 4 (Figure 6c). This is interesting to note since the A24a cortex represents the intersection of dorsal, ventral, and rostral areas. Indeed, in A25, as well as A32, the relative predominance of EC over dPMC emerges (Figure 6d,e). In A25, there were significantly more inputs from the EC compared to both AMY and dPMC ($F(2,11) = 18.02$, $p < .01$; Tukey's post-hoc, EC vs. AMY $p < .05$; EC vs. dPMC $p < 0.01$), especially in layers 2–3 where there was a relative peak in the density of EC terminations (Figure 6d). A32 inputs showed no significant differences between pathways.

A similar dorso-ventral shift was seen for retrograde-labeled projection neurons (outputs)—which exhibited a predominance of dPMC outputs from the dACC (A24b,c), while a predominance of EC outputs arose from the vACC (A24a and deep layers of A25) (Figure 6a-e, right). In A24a (Figure 6c; $F(2,11) = 4.957$, $p < .05$), there were significantly more projection neurons to the EC than to the dPMC (Tukey's post-hoc, $p < .05$). In A25 (Figure 6d), there were significantly more projection neurons to the EC compared to both dPMC and AMY ($F(2,11) = 10.48$, $p < .01$; Tukey's post-hoc, EC vs. AMY $p < .05$; EC vs. dPMC $p < .01$). On the other hand, A24b (Figure 6b; $F(2,11) = 9.017$, $p < .01$) and A24c (Figure 6a; $F(2,11) = 6.204$, $p < .05$) had significantly more projection neurons to the dPMC than to the EC (Tukey's post-hoc A24b: $p < .01$; A24c: $p < .05$). A32 outputs showed no significant differences between pathways.

Using dual immunofluorescence confocal imaging to visualize the regional and laminar overlaps in the pathways, we confirmed these laminar relationships and input-output overlap (Figure 6f,g). Consistent with the quantitative data in A24c, AMY inputs were denser in the upper layers, while dPMC inputs were denser in deep layers, overlapping with L5 AMY and dPMC projection neurons (Figure 6f). In A25 and A24a, we found strong overlap of AMY and EC inputs and outputs across all layers (Figure 6g). AMY and EC terminations in A25

in particular were heavily co-mingled in L1, but there was a relative increase in EC terminations in L2–3 (Figure 6d,g).

3.6 | Input/output relationships of EC, AMY, and dPMC pathways within ACC

To determine whether anterograde-labeled axon terminals (inputs) and retrograde-labeled projection neurons (outputs) for each injection site were correlated, we performed linear regression analyses (Pearson's correlation) on normalized densities of axon terminals and projection neurons in each ACC subregion. We found that, for each injection site, the relative regional density of input and output were significantly correlated. The ACC areas that received the densest labeled axon terminals (input) from each injection site also sends the densest labeled projection neurons (output) to each injection site. Interestingly, this input–output correlation was significant and strong only for the corticocortical ACC connections with the dPMC ($R = 0.87$, $p < .001$) and EC ($R = 0.87$, $p < 1.0e\text{-}4$), but not for ACC connections with the AMY ($R = 0.49$, $p = .07$; Figure 7a). We then assessed the input–output relationship across the different ACC connections with EC, dPMC, and AMY in cases with two or more injections in the same hemisphere. In this analysis, we only found a significant negative correlation between EC input to deep layers of the ACC and deep layer output to the dPMC ($R = -0.67$, $p < .01$; Figure 7b).

We ran further multivariate analyses to understand how ACC areas are similar to each other based on the relative overlap of EC, dPMC, and AMY connections. First, we plotted the relative density of projection neurons (outputs) to one injection site versus the other. While we did not find significant linear correlations, the scatter plots show that rostral, ventral, and dorsal ACC areas were clustered based on the overlap of EC, dPMC, and AMY projection neurons (Figure 7c-e). Thus, we assessed the clustering of ACC areas considering multiple outcome variables based on the regional and laminar distribution of EC, dPMC, and AMY interconnections using non-metric multidimensional scaling (NMDS), as described previously (Dombrowski, Hilgetag, & Barbas, 2001; Gilman, Medalla, & Luebke, 2017; Hilgetag, Burns, O'Neill, Scannell, & Young, 2000; Hsu, Luebke, & Medalla, 2017; Young et al., 1995) (Figure 7f). The NDMS plot clusters data points based on a proximity distance matrix of pair-wise correlations of each ACC area from each case such that data points that are closer together are more similar with respect to the set of outcome measures. NMDS analyses showed the clustering of each ACC area from multiple cases were broadly grouped into rostral (A32), ventral (A25, A24a) and dorsal (A24b,c) subdivisions. This indicates that dorsal A24b and A24c are more similar to each other, compared to the other ACC areas. A32, A24a, and A25 each form separate clusters that are relatively dissimilar (separated) from each other. Interestingly, the relative proximity of these areas follows the density gradient of dPMC and EC connections, with A24a closer to the dACC cluster than A25, the area with the least dPMC but the most EC connections. These regression, scatter plot, and unsupervised clustering NMDS analyses confirm our findings in the MANOVA, showing that dorsal and ventral ACC areas form discrete anatomical sectors with distinct dPMC and EC connection patterns.

4 | DISCUSSION

The ACC is a key structure involved in decision-making tasks that rely on motor, contextual, and motivational information from ongoing and past events (Botvinick et al., 2004; Braver, Reynolds, & Donaldson, 2003; Brown & Braver, 2008; Ito et al., 2003; Johnston et al., 2007; Kaping, Vinck, Hutchison, Everling, & Womelsdorf, 2011; MacDonald III, Cohen, Stenger, & Carter, 2000). As summarized in Figure 8, our study reveals robust anatomical segregation between dorsal (A24b,c) dPMC-related and ventral (A24a, A25) EC-related ACC circuits. However, the AMY has strong bidirectional connections across both ventral and dorsal ACC, interfacing with both the memory-related EC and premotor planning dPMC circuits. Among all ACC areas, the rACC (A32) had the lowest the relative density of the inter-connections with EC, dPMC, and AMY. The EC and AMY have strong bidirectional connections with the vACC (A25), where contextual and emotional memory is likely integrated. The vACC, along with deep layers of dACC (A24b,c) and—to a lesser extent—rACC (A32), sends a substantial projection to the AMY. The inputs from segregated ACC areas potentially converge in the AMY, and project back to the dACC (A24b,c) to integrate contextual and emotional memory information with goal-directed action.

4.1 | Distinct input–output relationships of ACC connections with entorhinal cortex

Our data reveal regional and laminar specificity of ACC connections with the EC. The EC is a major hub linking the hippocampus and the rest of the cortex, and is therefore critical in hippocampal-mediated long-term contextual and episodic memory functions (Canto, Wouterlood, & Witter, 2008; Eichenbaum & Lipton, 2008; Hinman et al., 2018; Killian et al., 2012; Sasaki et al., 2015; review: Suzuki & Amaral, 2004; Witter, Van Hoesen, & Amaral, 1989). Here we show that among ACC areas, the anterior EC has the strongest bidirectional connections with the vACC A25. In contrast, these connections are relatively weak in the dACC and rACC.

The laminar pattern of ACC projection neurons directed to the EC differed based on specific region or origin. The projection neurons from the vACC, specifically A25, directed to the EC mainly arise from deep layers (Figure 7). In contrast, projection neurons directed to the EC arising in the rACC A32, albeit not as dense, are predominantly found in the upper layers. Previous work studying labeled terminations in the EC show that projection neurons from A32 terminated in both upper and deep layers, while projection neurons from A25 terminated predominantly in the deep layers of the EC (Anderson et al., 2016; Bunce & Barbas, 2011; Insausti & Amaral, 2008; Joyce & Barbas, 2018; Mohedano-Moriano et al., 2007; Munoz & Insausti, 2005; Saleem et al., 2008). The laminar targets of the ACC projections to the EC may dictate how they can interact with downstream entorhinal pathways to and from the hippocampus and other cortical areas (review: Canto et al., 2008). The upper layers 2–3 of the EC project to the hippocampus, and, together with perirhinal and parahippocampal cortices, provides the major cortical input to the hippocampus (Saunders et al., 1988; Witter et al., 1989; Witter et al., 2000). In contrast, deep layers 5–6 of EC receive strong hippocampal input and, in turn, project to other cortical areas as the major hippocampal output (Blatt et al., 2003; Blatt & Rosene, 1988; Carmichael & Price, 1995; Insausti & Amaral, 2008; Insausti et al., 1987; Kondo et al., 2005; Lavenex & Amaral, 2000;

Mohedano-Moriano et al., 2007; Munoz & Insausti, 2005; Rosene & Van Hoesen, 1977; G. Van Hoesen & Pandya, 1975) (review: Canto et al., 2008). Hence, A25 projections terminating in the deep layers of the EC could exert a strong gating influence on downstream cortical pathways (Joyce & Barbas, 2018). On the other hand, the A32 projections to the EC, although relatively weaker than A25 projections, may influence EC outputs to other areas, as well as gate information to and from the hippocampus (Anderson et al., 2016; Bunce, Zikopoulos, Feinberg, & Barbas, 2013) (review: Barbas et al., 2012; Canto et al., 2008; de Curtis & Pare, 2004).

Although, given the contributions of local inter-laminar connections within the EC (Ohara et al., 2018), it is difficult to predict the specific functional effect of the laminar ACC connections with the EC shown here without further physiological and computational studies. Nevertheless, previous physiological stimulation experiments in rodents have shown that medial prefrontal inputs to the EC and perirhinal cortex drive feedforward information flow into the hippocampus (Paz et al., 2007; Paz, Pelletier, Bauer, & Pare, 2006; Witter et al., 2000) (review: Canto et al., 2008; de Curtis & Pare, 2004). A32 projections to the EC output layers to the hippocampus is also particularly interesting based on the fact that A32 has strong bidirectional interactions with the lateral prefrontal cortex, and is an important hub for cognitive control circuits (Barbas & Pandya, 1989; Kim et al., 2018; Medalla & Barbas, 2009, 2010, 2012; Tang et al., 2019). This EC inter-connection with A32 is perhaps the substrate by which long-term episodic or contextual memory processed within entorhinal-hippocampal circuits (review: Eichenbaum, 2017) can influence working memory networks for cognition and decision making, and vice versa.

4.2 | Ventral ACC integrates amygdala and medial temporal information

Bidirectional EC connections with the vACC A25 overlapped strongly with bidirectional AMY connections within both upper and deep layers. In particular, we show that the overlap of EC and AMY terminations were especially strong in L1. However, we found a peak of EC terminations in L2–3 that is relatively more dense than AMY terminations. Interestingly, previous anatomical work showed that L2–3 of the vACC are also heavily innervated by the hippocampus (Aggleton, Wright, Rosene, & Saunders, 2015), suggesting the vACC has the ability to integrate EC inputs with direct AMY and hippocampal inputs in a laminar specific manner. The reciprocal vACC projection neurons to EC and AMY emanate strongly from the deep layers of A25. These data suggest that the deep layers of A25 can send coordinated output to both the EC and AMY, which are also inter-connected with each other (Hoistad & Barbas, 2008; Saunders et al., 1988; Saunders & Rosene, 1988).

The EC is thought to be an important gateway for information flow between the cortex and the hippocampus, playing a role in encoding contextual and episodic memories (review: Eichenbaum, 2017) and learning novel reward associations (Buckmaster, Eichenbaum, Amaral, Suzuki, & Rapp, 2004; Sugase-Miyamoto & Richmond, 2007; Yang et al., 2014). Further, the EC and AMY provide strong input to the hippocampus (Blatt & Rosene, 1988; Fudge et al., 2012; Insausti et al., 1987; Mohedano-Moriano et al., 2007; Rosene & Van Hoesen, 1977; Suzuki & Amaral, 2004; Wang & Barbas, 2018), which, in turn, only sends unidirectional input to ACC (Barbas & Blatt, 1995; Saunders et al., 1988). Thus, the vACC

can influence intrinsic hippocampal processing via its output to both the AMY and the EC. Interestingly, both ACC and AMY are thought to gate information flow to and from the hippocampus via EC connections to enhance hippocampal dependent learning (review: Barbas et al., 2012; Canto et al., 2008; de Curtis & Pare, 2004; Killian et al., 2012; Koganezawa, Gisetstad, Husby, Doan, & Witter, 2015; Paz et al., 2007; Paz et al., 2006; Witter et al., 2000). In addition, direct vACC projections to the AMY play a role in modulating emotional learning and memory (Etkin, Egner, Peraza, Kandel, & Hirsch, 2006; Ghashghaei, Hilgetag, & Barbas, 2007; John, Bullock, Zikopoulos, & Barbas, 2013; Passamonti et al., 2008; Toyoda et al., 2011) (review: Etkin et al., 2011). In monkeys and humans, activity in the vACC has been specifically associated with autonomic arousal, pain, and negative valence (Critchley, Tang, Glaser, Butterworth, & Dolan, 2005; Ichikawa et al., 2011; Mohanty et al., 2007; Monosov & Hikosaka, 2012; Onoda et al.; Rudebeck et al., 2014; Wallis & Kennerley, 2011; Wang, Chen, & Yue, 2017). Moreover, the vACC in humans has been strongly implicated in major depressive disorders (e.g., Drevets et al., 2008; Rauch et al., 2006; Workman et al., 2016). Thus, the overlap of EC and AMY pathways within the vACC suggest a role in influencing information flow along hippocampal-rhinal cortex circuits to integrate emotional cues with contextual information.

4.3 | Overlap and laminar specificity of motor and amygdala connections in dACC

Our data reveal that the distinct ACC subregions differ with regard to the relative density of EC versus dPMC connections. While the vACC has stronger EC than dPMC connections, the dACC shows the opposite pattern, having strong dPMC but weak EC connections, consistent with previous work (Morecraft et al., 2012). Here we show that the robust dPMC projection neurons in the dACC predominantly arise from the deep layers and overlap with projection neurons to the AMY. Interestingly, previous work has shown that A24c in the dACC is strongly connected with the more posterior cingulate motor areas (Morecraft et al., 2012), which also have robust AMY connections (Morecraft et al., 2007), forming a network thought to be important for emotional and social motor expression (Livneh, Resnik, Shohat, & Paz, 2012; Morecraft et al., 2007). The laminar overlap of motor and emotional circuits in the dACC, specifically, is consistent with its role in mediating the aversive and motivational components (e.g., error and reward) of decision making (Bernacchia, Seo, Lee, & Wang, 2011; Feroz, Leicht, Steinmann, Andreou, & Mulert, 2017; Seo & Lee, 2007; Wittmann et al., 2016).

Although AMY and dPMC projection neurons both emanate from the deep layers of the dACC, terminations from these two structures predominantly target distinct layers; AMY terminations are found mainly in the upper layers 1–3, while dPMC terminations are found in the middle-deep layers 4–6. Thus, dPMC terminations overlap with cell bodies and proximal dendritic segments of dPMC and AMY-directed projection neurons, presumably providing “feedforward” or “driving” inputs (Abbott & Chance, 2005; Barbas, 2015; Felleman & Van Essen, 1991; Sherman & Guillery, 2002). In contrast, AMY terminations located in the upper layers, likely target distal dendrites of these neurons, consistent with “feedback” or “modulatory” inputs. Thus, if AMY and dPMC inputs targeted the same neurons, they would be segregated by dendritic compartments. It is known that processing within upper versus deep layers, and inputs in distal versus proximal dendrites, can have

distinct temporal dynamics of integration (Chandrasekaran, Peixoto, Newsome, & Shenoy, 2017; Hill, Varga, Jia, Sakmann, & Konnerth, 2013; Kerlin et al., 2019; Sajad, Godlove, & Schall, 2019); (review: Branco & Hausser, 2011; Magee, 2000; Major, Larkum, & Schiller, 2013; Spruston, 2008; Williams & Stuart, 2003).

Future empirical and computational studies are needed to assess the functional effects of the cellular and laminar compartmentalization of these inputs. For instance, a dendritic arrangement of distal AMY versus proximal dPMC inputs in A24c suggest a circuit configuration well poised for spike-timing dependent plasticity (Magee, 2000; Spruston, 2008) to perhaps facilitate associative learning of these two inputs. The overlap of dPMC input with proximal segments of AMY projection neurons, suggest a connection well suited for the on-going performance monitoring functions of the dACC (review: Branco & Hausser, 2011; Magee, 2000; Spruston, 2008; Williams & Stuart, 2003). Further, the dense AMY inputs in L1 overlap with distal dendrites, and this connection allows for longer integration times and dendritic plasticity to play a role in input–output transformation (Branco & Hausser, 2011; e.g., Hill et al., 2013; Kerlin et al., 2019; Magee, 2000; review: Major et al., 2013; Spruston, 2008; Williams & Stuart, 2003). While speculative, the diverse laminar patterns of these inputs have important implications on the temporal processing of signals at the cellular and network levels.

Consistent with these diverse laminar patterns of dPMC and AMY connections, at the functional level, the dACC is thought to be involved in both rapid and long integrative timescales of processing value-guided decisions—updating short term ongoing actions with past affective information on error and reward history (Cai & Padoa-Schioppa, 2012; Hunt et al., 2012; Kolling et al., 2016; Quilodran, Rothe, & Procyk, 2008; Rudebeck et al., 2008; Tsujimoto, Shimazu, Isomura, & Sasaki, 2010; Wittmann et al., 2016). Activity in the dACC has been associated with on-line error-monitoring and correction (Amemori & Graybiel, 2012; Godlove et al., 2011; Ito et al., 2003; Niki & Watanabe, 1979; Vogt, 2005). Further, *in vivo* data from monkeys suggest the dACC may be involved in the expression and maintenance of aversive memories, with decreased excitability in dACC preventing spontaneous recovery of aversive memories after fear extinction (Klavir, Genud-Gabai, & Paz, 2012). In addition to error signals, neuronal activity in the primate dACC encodes reward history, sending value signals based on previously chosen rewards (Bernacchia et al., 2011; Braver et al., 2003; Brown & Braver, 2008; Hunt et al., 2012; John et al., 2013; Kaping et al., 2011; Kolling et al., 2016; Seo & Lee, 2007; Shidara & Richmond, 2002; Wittmann et al., 2016). Therefore, the AMY may be sending information on previously learned reward values, which could then be integrated in the dACC to influence ongoing behavior and plan future actions. For instance, it has been shown in a decision-making task in monkeys that dACC neurons were responsive to movement initiation and direction before the trials, while vACC neurons were active after the reward (Cai & Padoa-Schioppa, 2012). This temporal dynamic found *in vivo* is consistent with a role of the vACC in integrating responses to rewards that can, in turn, be relayed directly—or indirectly via the AMY—to the dACC for reward history evaluations. Our data show the laminar segregation of incoming motor and affective information in the dACC that may contribute to the dynamic timescales for integration in these networks (Chandrasekaran et al., 2017; Murray et al., 2014; Procyk, Tanaka, & Joseph, 2000; Quilodran et al., 2008; Sajad et al., 2019).

5 | CONCLUSION

In summary, the data presented here show highly segregated inter-connections within the ACC consisting of entorhinal-related ventral networks and motor-planning dorsal networks. Further, our data show that the AMY, which is critical for emotional processing (Phelps & Anderson, 1997) (for review see Phelps & LeDoux, 2005; Yang & Wang, 2017), serves as a common integrator of these ACC networks, with laminar patterns that can support dynamic processing timescales. The vACC is in a position to integrate EC with AMY inputs and provide output to these structures from both upper and deep cortical layers. In contrast, dPMC and AMY connections are integrated across distinct layers of the dACC, highlighting laminar-specific dynamics of dACC motor and limbic circuits. The laminar circuit properties shown here will help inform functional network models to predict how these specific medial temporal and premotor ACC circuits are disrupted in affective and mood disorders.

ACKNOWLEDGMENTS

Bethany Bowley for help with anesthesia and surgeries; Alexander Hsu, Caroline Beneville, Alexandra Tsolias, Wayne Chang, Eli Shobin, Penny Schultz, Ajay Uprety, Katelyn Trecartin, Karen Bottenfield, Karen Slater and Veronica Go for technical help during post-op care and brain cutting.

Funding information

National Institute of Health (NIH), National Institute of Mental Health (NIMH), Grant/Award Numbers: K99/R00MH101234, R01/MH116008

DATA AVAILABILITY STATEMENT

The raw data that support the findings in this study are available from the corresponding author upon request.

Abbreviations:

AMY	amygdala
dACC	dorsal anterior cingulate cortex
dPMC	dorsal premotor cortex
EC	entorhinal cortex
rACC	rostral anterior cingulate cortex
vACC	ventral anterior cingulate cortex

REFERENCES

Abbott LF, & Chance FS (2005). Drivers and modulators from push-pull and balanced synaptic input. Progress in Brain Research, 149, 147–155. 10.1016/S0079-6123(05)49011-1 [PubMed: 16226582]

Aggleton JP, Wright NF, Rosene DL, & Saunders RC (2015). Complementary patterns of direct amygdala and hippocampal projections to the macaque prefrontal cortex. Cerebral Cortex, 25(11), 4351–4373. 10.1093/cercor/bhv019 [PubMed: 25715284]

Amatrudo JM, Weaver CM, Crimins JL, Hof PR, Rosene DL, & Luebke JI (2012). Influence of highly distinctive structural properties on the excitability of pyramidal neurons in monkey visual and

prefrontal cortices. The Journal of Neuroscience, 32(40), 13644–13660. 10.1523/JNEUROSCI.2581-12.2012 [PubMed: 23035077]

Amemori K, & Graybiel AM (2012). Localized microstimulation of primate pregenual cingulate cortex induces negative decision-making. Nature Neuroscience, 15(5), 776–785. 10.1038/nn.3088 [PubMed: 22484571]

Anderson MC, Bunce JG, & Barbas H (2016). Prefrontal-hippocampal pathways underlying inhibitory control over memory. Neurobiology of Learning and Memory, 134(Pt A), 145–161. 10.1016/j.nlm.2015.11.008 [PubMed: 26642918]

Barbas H (1995). Anatomic basis of cognitive-emotional interactions in the primate prefrontal cortex. Neuroscience and Biobehavioral Reviews, 19(3), 499–510. 10.1016/0149-7634(94)00053-4 [PubMed: 7566750]

Barbas H (2015). General cortical and special prefrontal connections: Principles from structure to function. Annual Review of Neuroscience, 38, 269–289. 10.1146/annurev-neuro-071714-033936

Barbas H, & Blatt GJ (1995). Topographically specific hippocampal projections target functionally distinct prefrontal areas in the rhesus monkey. Hippocampus, 5, 511–533. [PubMed: 8646279]

Barbas H, Bunce JG, & Medalla M (2012). Prefrontal pathways that control attention. In Stuss DTK, T. R (Ed.), Principles of frontal lobe function (2nd ed.). New York: Oxford University Press.

Barbas H, & De Olmos J (1990). Projections from the amygdala to basoventral and mediodorsal prefrontal regions in the rhesus monkey. Journal of Comparative Neurology, 300(4), 549–571.

Barbas H, & Pandya DN (1987). Architecture and frontal cortical connections of the premotor cortex (area 6) in the rhesus monkey. The Journal of Comparative Neurology, 256(2), 211–228. 10.1002/cne.902560203 [PubMed: 3558879]

Barbas H, & Pandya DN (1989). Architecture and intrinsic connections of the prefrontal cortex in the rhesus monkey. The Journal of Comparative Neurology, 286(3), 353–375. 10.1002/cne.902860306 [PubMed: 2768563]

Barbas H, Saha S, Rempel-Clower N, & Ghashghaei T (2003). Serial pathways from primate prefrontal cortex to autonomic areas may influence emotional expression. BMC Neuroscience, 4(1), 25. [PubMed: 14536022]

Barbas H, & Zikopoulos B (2007). The prefrontal cortex and flexible behavior. The Neuroscientist, 13(5), 532–545. 10.1177/1073858407301369 [PubMed: 17901261]

Bates JF, & Goldman-Rakic PS (1993). Prefrontal connections of medial motor areas in the rhesus monkey. Journal of Comparative Neurology, 336, 211–228.

Bernacchia A, Seo H, Lee D, & Wang XJ (2011). A reservoir of time constants for memory traces in cortical neurons. Nature Neuroscience, 14(3), 366–372. 10.1038/nn.2752 [PubMed: 21317906]

Blatt GJ, Pandya DN, & Rosene DL (2003). Parcellation of cortical afferents to three distinct sectors in the parahippocampal gyrus of the rhesus monkey: An anatomical and neurophysiological study. Journal of Comparative Neurology, 466(2), 161–179.

Blatt GJ, & Rosene DL (1988). Organization of hippocampal efferent projections to the cerebral cortex in the rhesus monkey. Neuroscience Abstracts, 14, 859.

Botvinick MM, Cohen JD, & Carter CS (2004). Conflict monitoring and anterior cingulate cortex: An update. Trends in Cognitive Sciences, 8(12), 539–546. [PubMed: 15556023]

Branco T, & Hausser M (2011). Synaptic integration gradients in single cortical pyramidal cell dendrites. Neuron, 69(5), 885–892. 10.1016/j.neuron.2011.02.006 [PubMed: 21382549]

Braver TS, Reynolds JR, & Donaldson DI (2003). Neural mechanisms of transient and sustained cognitive control during task switching. Neuron, 39(4), 713–726. [PubMed: 12925284]

Brown JW, & Braver TS (2008). A computational model of risk, conflict, and individual difference effects in the anterior cingulate cortex. Brain Research, 1202, 99–108. [PubMed: 17707352]

Buckmaster CA, Eichenbaum H, Amaral DG, Suzuki WA, & Rapp PR (2004). Entorhinal cortex lesions disrupt the relational organization of memory in monkeys. The Journal of Neuroscience, 24(44), 9811–9825. 10.1523/JNEUROSCI.1532-04.2004 [PubMed: 15525766]

Bunce JG, & Barbas H (2011). Prefrontal pathways target excitatory and inhibitory systems in memory-related medial temporal cortices. NeuroImage, 55(4), 1461–1474. [PubMed: 21281716]

Bunce JG, Zikopoulos B, Feinberg M, & Barbas H (2013). Parallel prefrontal pathways reach distinct excitatory and inhibitory systems in memory-related rhinal cortices. The Journal of Comparative Neurology, 521(18), 4260–4283. 10.1002/cne.23413 [PubMed: 23839697]

Bush G, Luu P, & Posner MI (2000). Cognitive and emotional influences in anterior cingulate cortex. Trends in Cognitive Sciences, 4 (6), 215–222. [PubMed: 10827444]

Cai X, & Padoa-Schioppa C (2012). Neuronal encoding of subjective value in dorsal and ventral anterior cingulate cortex. The Journal of Neuroscience, 32(11), 3791–3808. 10.1523/JNEUROSCI.3864-11.2012 [PubMed: 22423100]

Canto CB, Wouterlood FG, & Witter MP (2008). What does the anatomical organization of the entorhinal cortex tell us? Neural Plasticity, 2008, 381243. 10.1155/2008/381243, 1, 18 [PubMed: 18769556]

Carmichael ST, & Price JL (1995). Sensory and premotor connections of the orbital and medial prefrontal cortex of macaque monkeys. Journal of Comparative Neurology, 363, 642–664.

Chandrasekaran C, Peixoto D, Newsome WT, & Shenoy KV (2017). Laminar differences in decision-related neural activity in dorsal premotor cortex. Nature Communications, 8(1), 614. 10.1038/s41467-017-00715-0

Critchley HD, Tang J, Glaser D, Butterworth B, & Dolan RJ (2005). Anterior cingulate activity during error and autonomic response. NeuroImage, 27(4), 885–895. 10.1016/j.neuroimage.2005.05.047 [PubMed: 15996878]

de Curtis M, & Pare D (2004). The rhinal cortices: A wall of inhibition between the neocortex and the hippocampus. Progress in Neurobiology, 74(2), 101–110. 10.1016/j.pneurobio.2004.08.005 [PubMed: 15518955]

Dombrowski SM, Hilgetag CC, & Barbas H (2001). Quantitative architecture distinguishes prefrontal cortical systems in the rhesus monkey. Cerebral Cortex, 11(10), 975–988. 10.1093/cercor/11.10.975 [PubMed: 11549620]

Drevets WC, Savitz J, & Trimble M (2008). The subgenual anterior cingulate cortex in mood disorders. CNS Spectrums, 13(8), 663–681. 10.1017/s1092852900013754 [PubMed: 18704022]

Dum RP, & Strick PL (1992). Medial wall motor areas and skeletomotor control. Current Opinion in Neurobiology, 2, 836–839. [PubMed: 1477548]

Dum RP, & Strick PL (2002). Motor areas in the frontal lobe of the primate. Physiology & Behavior, 77(4–5), 677–682. [PubMed: 12527018]

Eichenbaum H (2017). On the integration of space, time, and memory. Neuron, 95(5), 1007–1018. 10.1016/j.neuron.2017.06.036 [PubMed: 28858612]

Eichenbaum H, & Lipton PA (2008). Towards a functional organization of the medial temporal lobe memory system: Role of the parahippocampal and medial entorhinal cortical areas. Hippocampus, 18 (12), 1314–1324. 10.1002/hipo.20500 [PubMed: 19021265]

Etkin A, Egner T, & Kalisch R (2011). Emotional processing in anterior cingulate and medial prefrontal cortex. Trends in Cognitive Sciences, 15 (2), 85–93. 10.1016/j.tics.2010.11.004 [PubMed: 21167765]

Etkin A, Egner T, Peraza DM, Kandel ER, & Hirsch J (2006). Resolving emotional conflict: A role for the rostral anterior cingulate cortex in modulating activity in the amygdala. Neuron, 51(6), 871–882. 10.1016/j.neuron.2006.07.029 [PubMed: 16982430]

Felleman DJ, & Van Essen DC (1991). Distributed hierarchical processing in the primate cerebral cortex. Cerebral Cortex, 1(1), 1–47. 10.1093/cercor/1.1.1 [PubMed: 1822724]

Feroz FS, Leicht G, Steinmann S, Andreou C, & Mulert C (2017). The time course of activity within the dorsal and rostral-ventral anterior cingulate cortex in the emotional Stroop task. Brain Topography, 30(1), 30–45. 10.1007/s10548-016-0521-3 [PubMed: 27659288]

Fudge JL, deCampo DM, & Becoats KT (2012). Revisiting the hippocampal-amygdala pathway in primates: Association with immature-appearing neurons. Neuroscience, 212, 104–119. 10.1016/j.neuroscience.2012.03.040 [PubMed: 22521814]

Ghashghaei HT, & Barbas H (2002). Pathways for emotion: Interactions of prefrontal and anterior temporal pathways in the amygdala of the rhesus monkey. Neuroscience, 115(4), 1261–1279. 10.1016/s0306-4522(02)00446-3 [PubMed: 12453496]

Ghashghaei HT, Hilgetag CC, & Barbas H (2007). Sequence of information processing for emotions based on the anatomic dialogue between prefrontal cortex and amygdala. NeuroImage, 34(3), 905–923. 10.1016/j.neuroimage.2006.09.046 [PubMed: 17126037]

Gilman JP, Medalla M, & Luebke JI (2017). Area-specific features of pyramidal neurons-a comparative study in mouse and rhesus monkey. Cerebral Cortex, 27(3), 2078–2094. 10.1093/cercor/bhw062 [PubMed: 26965903]

Godlove DC, Emeric EE, Segovis CM, Young MS, Schall JD, & Woodman GF (2011). Event-related potentials elicited by errors during the stop-signal task. I. Macaque monkeys. The Journal of Neuroscience, 31(44), 15640–15649. 10.1523/JNEUROSCI.3349-11.2011 [PubMed: 22049407]

Hayden BY, & Platt ML (2010). Neurons in anterior cingulate cortex multiplex information about reward and action. The Journal of Neuroscience, 30(9), 3339–3346. 10.1523/JNEUROSCI.4874-09.2010 [PubMed: 20203193]

Hilgetag CC, Burns GA, O'Neill MA, Scannell JW, & Young MP (2000). Anatomical connectivity defines the organization of clusters of cortical areas in the macaque monkey and the cat. Philosophical Transactions of the Royal Society of London. Series B, Biological Sciences, 355 (1393), 91–110. 10.1098/rstb.2000.0551 [PubMed: 10703046]

Hilgetag CC, Medalla M, Beul SF, & Barbas H (2016). The primate connectome in context: Principles of connections of the cortical visual system. NeuroImage, 134, 685–702. 10.1016/j.neuroimage.2016.04.017 [PubMed: 27083526]

Hill DN, Varga Z, Jia H, Sakmann B, & Konnerth A (2013). Multi-branch activity in basal and tuft dendrites during firing of layer 5 cortical neurons in vivo. Proceedings of the National Academy of Sciences of the United States of America, 110(33), 13618–13623. 10.1073/pnas.1312599110 [PubMed: 23904480]

Hinman JR, Dannenberg H, Alexander AS, & Hasselmo ME (2018). Neural mechanisms of navigation involving interactions of cortical and subcortical structures. Journal of Neurophysiology, 119(6), 2007–2029. 10.1152/jn.00498.2017 [PubMed: 29442559]

Hoistad M, & Barbas H (2008). Sequence of information processing for emotions through pathways linking temporal and insular cortices with the amygdala. NeuroImage, 40(3), 1016–1033. 10.1016/j.neuroimage.2007.12.043 [PubMed: 18261932]

Hsu A, Luebke JI, & Medalla M (2017). Comparative ultrastructural features of excitatory synapses in the visual and frontal cortices of the adult mouse and monkey. The Journal of Comparative Neurology, 525 (9), 2175–2191. 10.1002/cne.24196 [PubMed: 28256708]

Hunt LT, Kolling N, Soltani A, Woolrich MW, Rushworth MF, & Behrens TE (2012). Mechanisms underlying cortical activity during value-guided choice. Nature Neuroscience, 15(3), 470–476, S471–473. 10.1038/nn.3017 [PubMed: 22231429]

Ichikawa N, Siegle GJ, Jones NP, Kamishima K, Thompson WK, Gross JJ, & Ohira H (2011). Feeling bad about screwing up: Emotion regulation and action monitoring in the anterior cingulate cortex. Cognitive, Affective, & Behavioral Neuroscience, 11(3), 354–371. 10.3758/s13415-011-0028-z

Insausti R, & Amaral DG (2008). Entorhinal cortex of the monkey: IV. Topographical and laminar organization of cortical afferents. The Journal of Comparative Neurology, 509(6), 608–641. 10.1002/cne.21753 [PubMed: 18551518]

Insausti R, Amaral DG, & Cowan WM (1987). The entorhinal cortex of the monkey: II. Cortical afferents. Journal of Comparative Neurology, 264, 356–395.

Ito S, Stuphorn V, Brown JW, & Schall JD (2003). Performance monitoring by the anterior cingulate cortex during saccade countermanding. Science, 302(5642), 120–122. [PubMed: 14526085]

Iwai E, & Yukie M (1987). Amygdalofugal and amygdalopetal connections with modality-specific visual cortical areas in macaques (*Macaca fuscata*, M. mulatta, and *M. fascicularis*). The Journal of Comparative Neurology, 261(3), 362–387. 10.1002/cne.902610304 [PubMed: 3611417]

John YJ, Bullock D, Zikopoulos B, & Barbas H (2013). Anatomy and computational modeling of networks underlying cognitive-emotional interaction. Frontiers in Human Neuroscience, 7, 101. 10.3389/fnhum.2013.00101 [PubMed: 23565082]

Johnston K, Levin HM, Koval MJ, & Everling S (2007). Top-down control-signal dynamics in anterior cingulate and prefrontal cortex neurons following task switching. Neuron, 53(3), 453–462. [PubMed: 17270740]

Joyce MKP, & Barbas H (2018). Cortical connections position primate area 25 as a keystone for Interoception, emotion, and memory. The Journal of Neuroscience, 38(7), 1677–1698. 10.1523/JNEUROSCI.2363-17.2017 [PubMed: 29358365]

Kaping D, Vinck M, Hutchison RM, Everling S, & Womelsdorf T (2011). Specific contributions of ventromedial, anterior cingulate, and lateral prefrontal cortex for attentional selection and stimulus valuation. PLoS Biology, 9(12), e1001224. 10.1371/journal.pbio.1001224 [PubMed: 22215982]

Kennerley SW, & Walton ME (2011). Decision making and reward in frontal cortex: Complementary evidence from neurophysiological and neuropsychological studies. Behavioral Neuroscience, 125(3), 297–317. 10.1037/a0023575 [PubMed: 21534649]

Kerlin A, Boaz M, Flickinger D, MacLennan BJ, Dean MB, Davis C, … Svoboda K (2019). Functional clustering of dendritic activity during decision-making. eLife, 8, e46966. 10.7554/eLife.46966 [PubMed: 31663507]

Killian NJ, Jutras MJ, & Buffalo EA (2012). A map of visual space in the primate entorhinal cortex. Nature, 491(7426), 761–764. 10.1038/nature11587 [PubMed: 23103863]

Kim Y, Sakata H, Nejime M, Konoike N, Miyachi S, & Nakamura K (2018). Afferent connections of the dorsal, perigenual, and subgenual anterior cingulate cortices of the monkey: Amygdalar inputs and intrinsic connections. Neuroscience Letters, 681, 93–99. 10.1016/j.neulet.2018.05.028 [PubMed: 29803854]

Klavir O, Genud-Gabai R, & Paz R (2012). Low-frequency stimulation depresses the primate anterior-cingulate-cortex and prevents spontaneous recovery of aversive memories. The Journal of Neuroscience, 32(25), 8589–8597. 10.1523/JNEUROSCI.6481-11.2012 [PubMed: 22723700]

Koganezawa N, Gisetstad R, Husby E, Doan TP, & Witter MP (2015). Excitatory Postrhinal projections to principal cells in the medial Entorhinal cortex. The Journal of Neuroscience, 35(48), 15860–15874. 10.1523/JNEUROSCI.0653-15.2015 [PubMed: 26631468]

Kolling N, Wittmann MK, Behrens TE, Boorman ED, Mars RB, & Rushworth MF (2016). Value, search, persistence and model updating in anterior cingulate cortex. Nature Neuroscience, 19(10), 1280–1285. 10.1038/nn.4382 [PubMed: 27669988]

Kondo H, Saleem KS, & Price JL (2005). Differential connections of the perirhinal and parahippocampal cortex with the orbital and medial prefrontal networks in macaque monkeys. Journal of Comparative Neurology, 493(4), 479–509.

Lavenex P, & Amaral DG (2000). Hippocampal-neocortical interaction: A hierarchy of associativity. Hippocampus, 10(4), 420–430. 10.1002/1098-1063(2000)10:4<420::AID-HIPO8>3.0.CO;2-5 [PubMed: 10985281]

Lavenex P, Suzuki WA, & Amaral DG (2002). Perirhinal and parahippocampal cortices of the macaque monkey: Projections to the neocortex. Journal of Comparative Neurology, 447(4), 394–420.

Livneh U, Resnik J, Shohat Y, & Paz R (2012). Self-monitoring of social facial expressions in the primate amygdala and cingulate cortex. Proceedings of the National Academy of Sciences of the United States of America, 109(46), 18956–18961. 10.1073/pnas.1207662109 [PubMed: 23112157]

Luppino G, Rozzi S, Calzavara R, & Matelli M (2003). Prefrontal and agranular cingulate projections to the dorsal premotor areas F2 and F7 in the macaque monkey. The European Journal of Neuroscience, 17(3), 559–578. 10.1046/j.1460-9568.2003.02476.x [PubMed: 12581174]

MacDonald AW III, Cohen JD, Stenger VA, & Carter CS (2000). Dissociating the role of the dorsolateral prefrontal and anterior cingulate cortex in cognitive control. Science, 288(5472), 1835–1838. [PubMed: 10846167]

Magee JC (2000). Dendritic integration of excitatory synaptic input. Nature Reviews. Neuroscience, 1(3), 181–190. 10.1038/35044552 [PubMed: 11257906]

Major G, Larkum ME, & Schiller J (2013). Active properties of neocortical pyramidal neuron dendrites. Annual Review of Neuroscience, 36, 1–24. 10.1146/annurev-neuro-062111-150343

Medalla M, & Barbas H (2009). Synapses with inhibitory neurons differentiate anterior cingulate from dorsolateral prefrontal pathways associated with cognitive control. Neuron, 61(4), 609–620. 10.1016/j.neuron.2009.01.006 [PubMed: 19249280]

Medalla M, & Barbas H (2010). Anterior cingulate synapses in prefrontal areas 10 and 46 suggest differential influence in cognitive control. The Journal of Neuroscience, 30(48), 16068–16081. 10.1523/JNEUROSCI.1773-10.2010 [PubMed: 21123554]

Medalla M, & Barbas H (2012). The anterior cingulate cortex may enhance inhibition of lateral prefrontal cortex via m2 cholinergic receptors at dual synaptic sites. The Journal of Neuroscience, 32(44), 15611–15625. 10.1523/JNEUROSCI.2339-12.2012 [PubMed: 23115196]

Medalla M, Gilman JP, Wang JY, & Luebke JI (2017). Strength and diversity of inhibitory signaling differentiates primate anterior cingulate from lateral prefrontal cortex. The Journal of Neuroscience, 37(18), 4717–4734. 10.1523/JNEUROSCI.3757-16.2017 [PubMed: 28381592]

Medalla M, Lera P, Feinberg M, & Barbas H (2007). Specificity in inhibitory systems associated with prefrontal pathways to temporal cortex in primates. Cerebral Cortex, 17(Suppl 1), i136–i150. 10.1093/cercor/bhm068 [PubMed: 17725996]

Mohanty A, Engels AS, Herrington JD, Heller W, Ho MH, Banich MT, … Miller GA (2007). Differential engagement of anterior cingulate cortex subdivisions for cognitive and emotional function. Psychophysiology, 44(3), 343–351. 10.1111/j.1469-8986.2007.00515.x [PubMed: 17433093]

Mohedano-Moriano A, Pro-Sistiaga P, Arroyo-Jimenez MM, Artacho-Perula E, Insausti AM, Marcos P, … Insausti R (2007). Topographical and laminar distribution of cortical input to the monkey entorhinal cortex. Journal of Anatomy, 211(2), 250–260. [PubMed: 17573826]

Monosov IE, & Hikosaka O (2012). Regionally distinct processing of rewards and punishments by the primate ventromedial prefrontal cortex. The Journal of Neuroscience, 32(30), 10318–10330. 10.1523/JNEUROSCI.1801-12.2012 [PubMed: 22836265]

Morecraft RJ, McNeal DW, Stilwell-Morecraft KS, Gedney M, Ge J, Schroeder CM, & van Hoesen GW (2007). Amygdala interconnections with the cingulate motor cortex in the rhesus monkey. The Journal of Comparative Neurology, 500(1), 134–165. 10.1002/cne.21165 [PubMed: 17099887]

Morecraft RJ, Stilwell-Morecraft KS, Cipolloni PB, Ge J, McNeal DW, & Pandya DN (2012). Cytoarchitecture and cortical connections of the anterior cingulate and adjacent somatomotor fields in the rhesus monkey. Brain Research Bulletin, 87(4–5), 457–497. 10.1016/j.brainresbull.2011.12.005 [PubMed: 22240273]

Munoz M, & Insausti R (2005). Cortical efferents of the entorhinal cortex and the adjacent parahippocampal region in the monkey (*Macaca fascicularis*). The European Journal of Neuroscience, 22(6), 1368–1388. 10.1111/j.1460-9568.2005.04299.x [PubMed: 16190892]

Murray JD, Bernacchia A, Freedman DJ, Romo R, Wallis JD, Cai X, … Wang XJ (2014). A hierarchy of intrinsic timescales across primate cortex. Nature Neuroscience, 17(12), 1661–1663. 10.1038/nn.3862 [PubMed: 25383900]

Niki H, & Watanabe M (1979). Prefrontal and cingulate unit activity during timing behavior in the monkey. Brain Research, 171, 213–224. [PubMed: 111772]

Ohara S, Onodera M, Simonsen OW, Yoshino R, Hioki H, Iijima T, … Witter MP (2018). Intrinsic projections of layer Vb neurons to layers Va, III, and II in the lateral and medial Entorhinal cortex of the rat. Cell Reports, 24(1), 107–116. 10.1016/j.celrep.2018.06.014 [PubMed: 29972772]

Onoda K, Okamoto Y, Nakashima K, Nittono H, Ura M, & Yamawaki S (2009). Decreased ventral anterior cingulate cortex activity is associated with reduced social pain during emotional support. Social Neuroscience, 4(5), 443–454. 10.1080/17470910902955884 [PubMed: 19562631]

Pandya DN, Van Hoesen GW, & Mesulam MM (1981). Efferent connections of the cingulate gyrus in the rhesus monkey. Experimental Brain Research, 42, 319–330. [PubMed: 6165607]

Passamonti L, Rowe JB, Ewbank M, Hampshire A, Keane J, & Calder AJ (2008). Connectivity from the ventral anterior cingulate to the amygdala is modulated by appetitive motivation in response to facial signals of aggression. NeuroImage, 43(3), 562–570. 10.1016/j.neuroimage.2008.07.045 [PubMed: 18722533]

Paus T (2001). Primate anterior cingulate cortex: Where motor control, drive and cognition interface. Nature Reviews Neuroscience, 2(6), 417–424. [PubMed: 11389475]

Paz R, Bauer EP, & Pare D (2007). Learning-related facilitation of rhinal interactions by medial prefrontal inputs. The Journal of Neuroscience, 27(24), 6542–6551. 10.1523/JNEUROSCI.1077-07.2007 [PubMed: 17567815]

Paz R, Pelletier JG, Bauer EP, & Pare D (2006). Emotional enhancement of memory via amygdala-driven facilitation of rhinal interactions. Nature Neuroscience, 9(10), 1321–1329. 10.1038/nn1771 [PubMed: 16964249]

Pessoa L (2010). Emergent processes in cognitive-emotional interactions. Dialogues in Clinical Neuroscience, 12(4), 433–448. [PubMed: 21319489]

Phelps EA (2004). Human emotion and memory: Interactions of the amygdala and hippocampal complex. Current Opinion in Neurobiology, 14(2), 198–202. [PubMed: 15082325]

Phelps EA, & Anderson AK (1997). Emotional memory: What does the amygdala do? Current Biology, 7(5), R311–R314. 10.1016/s0960-9822(06)00146-1 [PubMed: 9115384]

Phelps EA, & LeDoux JE (2005). Contributions of the amygdala to emotion processing: From animal models to human behavior. Neuron, 48(2), 175–187. 10.1016/j.neuron.2005.09.025 [PubMed: 16242399]

Pitkanen A, & Amaral DG (1994). The distribution of GABAergic cells, fibers, and terminals in the monkey amygdaloid complex: An immuno-histochemical and in situ hybridization study. The Journal of Neuroscience, 14(4), 2200–2224. [PubMed: 8158266]

Procyk E, Tanaka YL, & Joseph JP (2000). Anterior cingulate activity during routine and non-routine sequential behaviors in macaques. Nature Neuroscience, 3(5), 502–508. 10.1038/74880 [PubMed: 10769392]

Quilodran R, Rothe M, & Procyk E (2008). Behavioral shifts and action valuation in the anterior cingulate cortex. Neuron, 57(2), 314–325. 10.1016/j.neuron.2007.11.031 [PubMed: 18215627]

Rauch SL, Shin LM, & Phelps EA (2006). Neurocircuitry models of post-traumatic stress disorder and extinction: Human neuroimaging research—Past, present, and future. Biological Psychiatry, 60(4), 376–382. [PubMed: 16919525]

Reiner A, Veenman CL, Medina L, Jiao Y, Del Mar N, & Honig MG (2000). Pathway tracing using biotinylated dextran amines. Journal of Neuroscience Methods, 103(1), 23–37. 10.1016/s0165-0270(00)00293-4 [PubMed: 11074093]

Rempel-Clower NL, & Barbas H (2000). The laminar pattern of connections between prefrontal and anterior temporal cortices in the rhesus monkey is related to cortical structure and function. Cerebral Cortex, 10(9), 851–865. 10.1093/cercor/10.9.851 [PubMed: 10982746]

Rosene DL, Roy NJ, & Davis BJ (1986). A cryoprotection method that facilitates cutting frozen sections of whole monkey brains for histological and histochemical processing without freezing artifact. The Journal of Histochemistry and Cytochemistry, 34(10), 1301–1315. 10.1177/34.10.3745909 [PubMed: 3745909]

Rosene DL, & Van Hoesen GW (1977). Hippocampal efferents reach widespread areas of cerebral cortex and amygdala in the rhesus monkey. Science, 198, 315–317. [PubMed: 410102]

Rudebeck PH, Behrens TE, Kennerley SW, Baxter MG, Buckley MJ, Walton ME, & Rushworth MF (2008). Frontal cortex subregions play distinct roles in choices between actions and stimuli. The Journal of Neuroscience, 28(51), 13775–13785. 10.1523/JNEUROSCI.3541-08.2008 [PubMed: 19091968]

Rudebeck PH, Putnam PT, Daniels TE, Yang T, Mitz AR, Rhodes SE, & Murray EA (2014). A role for primate subgenual cingulate cortex in sustaining autonomic arousal. Proceedings of the National Academy of Sciences of the United States of America, 111(14), 5391–5396. 10.1073/pnas.1317695111 [PubMed: 24706828]

Sajad A, Godlove DC, & Schall JD (2019). Cortical microcircuitry of performance monitoring. Nature Neuroscience, 22(2), 265–274. 10.1038/s41593-018-0309-8 [PubMed: 30643297]

Saleem KS, Kondo H, & Price JL (2008). Complementary circuits connecting the orbital and medial prefrontal networks with the temporal, insular, and opercular cortex in the macaque monkey. The Journal of Comparative Neurology, 506(4), 659–693. 10.1002/cne.21577 [PubMed: 18067141]

Sasaki T, Leutgeb S, & Leutgeb JK (2015). Spatial and memory circuits in the medial entorhinal cortex. Current Opinion in Neurobiology, 32, 16–23. 10.1016/j.conb.2014.10.008 [PubMed: 25463560]

Saunders RC, & Rosene DL (1988). A comparison of the efferents of the amygdala and the hippocampal formation in the rhesus monkey: I. Convergence in the entorhinal, prorhinal, and

perirhinal cortices. The Journal of Comparative Neurology, 271(2), 153–184. 10.1002/cne.902710202 [PubMed: 2454246]

Saunders RC, Rosene DL, & Van Hoesen GW (1988). Comparison of the efferents of the amygdala and the hippocampal formation in the rhesus monkey: II. Reciprocal and non-reciprocal connections. The Journal of Comparative Neurology, 271(2), 185–207. 10.1002/cne.902710203 [PubMed: 2454247]

Schall JD, Morel A, & Kaas JH (1993). Topography of supplementary eye field afferents to frontal eye field in macaque: Implications for mapping between saccade coordinate systems. Visual Neuroscience, 10 (2), 385–393. 10.1017/s0952523800003771 [PubMed: 7683486]

Schmitz C, & Hof PR (2005). Design-based stereology in neuroscience. Neuroscience, 130(4), 813–831. 10.1016/j.neuroscience.2004.08.050 [PubMed: 15652981]

Seo H, & Lee D (2007). Temporal filtering of reward signals in the dorsal anterior cingulate cortex during a mixed-strategy game. The Journal of Neuroscience, 27(31), 8366–8377. 10.1523/JNEUROSCI.2369-07.2007 [PubMed: 17670983]

Sharma KK, Kelly EA, Pfeifer CW, & Fudge JL (2019). Translating fear circuitry: Amygdala projections to subgenual and perigenual anterior cingulate in the macaque. Cerebral Cortex, 30, 550–562. 10.1093/cercor/bhz106

Shen C, Ardid S, Kaping D, Westendorff S, Everling S, & Womelsdorf T (2015). Anterior cingulate cortex cells identify process-specific errors of Attentional control prior to transient prefrontal-cingulate inhibition. Cerebral Cortex, 25(8), 2213–2228. 10.1093/cercor/bhu028 [PubMed: 24591526]

Sherman SM, & Guillery RW (2002). The role of the thalamus in the flow of information to the cortex. Philosophical Transactions of the Royal Society of London. Series B, Biological Sciences, 357(1428), 1695–1708. 10.1098/rstb.2002.1161 [PubMed: 12626004]

Shidara M, & Richmond BJ (2002). Anterior cingulate: Single neuronal signals related to degree of reward expectancy. Science, 296(5573), 1709–1711. 10.1126/science.1069504 [PubMed: 12040201]

Spruston N (2008). Pyramidal neurons: Dendritic structure and synaptic integration. Nature Reviews. Neuroscience, 9(3), 206–221. 10.1038/nrn2286 [PubMed: 18270515]

Stevens FL, Hurley RA, & Taber KH (2011). Anterior cingulate cortex: unique role in cognition and emotion. The Journal of Neuropsychiatry and Clinical Neurosciences, 23(2), 121–125. 10.1176/appi.neuropsych.23.2.121 [PubMed: 21677237]

Sugase-Miyamoto Y, & Richmond BJ (2007). Cue and reward signals carried by monkey entorhinal cortex neurons during reward schedules. Experimental Brain Research, 181(2), 267–276. 10.1007/s00221-007-0926-z [PubMed: 17396249]

Suzuki WA, & Amaral DG (2004). Functional neuroanatomy of the medial temporal lobe memory system. Cortex, 40(1), 220–222. [PubMed: 15070014]

Tang W, Jbabdi S, Zhu Z, Cottaar M, Grisot G, Lehman JF, … Haber SN (2019). A connectional hub in the rostral anterior cingulate cortex links areas of emotion and cognitive control. eLife, 8, e43761. 10.7554/eLife.43761 [PubMed: 31215864]

Toyoda H, Li XY, Wu LJ, Zhao MG, Descalzi G, Chen T, … Zhuo M (2011). Interplay of amygdala and cingulate plasticity in emotional fear. Neural Plasticity, 2011, 1–9. 10.1155/2011/813749

Tsujimoto T, Shimazu H, Isomura Y, & Sasaki K (2010). Theta oscillations in primate prefrontal and anterior cingulate cortices in forewarned reaction time tasks. Journal of Neurophysiology, 103(2), 827–843. 10.1152/jn.00358.2009 [PubMed: 20007502]

Van Hoesen G, & Pandya DN (1975). Some connections of the entorhinal (area 28) and perirhinal (area 35) cortices of the rhesus monkey. I. Temporal lobe afferents. Brain Research, 95(1), 1–24. 10.1016/0006-8993(75)90204-8 [PubMed: 1156859]

Van Hoesen GW, M. RJ; Vogt BA (1993). Connections of the monkey cingulate cortex. In G. BA M. Vogt (Ed.), Neurobiology of cingulate cortex and limbic thalamus (pp. 249–284). Boston, MA: Birkhauser.

Veenman CL, Reiner A, & Honig MG (1992). Biotinylated dextran amine as an anterograde tracer for single- and double-labeling studies. Journal of Neuroscience Methods, 41(3), 239–254. 10.1016/0165-0270(92)90089-v [PubMed: 1381034]

Vogt BA (2005). Pain and emotion interactions in subregions of the cingulate gyrus. Nature Reviews Neuroscience, 6(7), 533–544. [PubMed: 15995724]

Wallis JD, & Kennerley SW (2011). Contrasting reward signals in the orbitofrontal cortex and anterior cingulate cortex. Annals of the new York Academy of Sciences, 1239, 33–42. 10.1111/j.1749-6632.2011.06277.x [PubMed: 22145873]

Wang J, & Barbas H (2018). Specificity of primate Amygdalar pathways to hippocampus. The Journal of Neuroscience, 38(47), 10019–10041. 10.1523/JNEUROSCI.1267-18.2018 [PubMed: 30249799]

Wang Y, Chen J, & Yue Z (2017). Positive emotion facilitates cognitive flexibility: An fMRI study. Frontiers in Psychology, 8, 1832. 10.3389/fpsyg.2017.01832 [PubMed: 29163255]

West MJ, Slomianka L, & Gundersen HJ (1991). Unbiased stereological estimation of the total number of neurons in thesubdivisions of the rat hippocampus using the optical fractionator. The Anatomical Record, 231(4), 482–497. 10.1002/ar.1092310411 [PubMed: 1793176]

Williams SR, & Stuart GJ (2003). Role of dendritic synapse location in the control of action potential output. Trends in Neurosciences, 26(3), 147–154. 10.1016/S0166-2236(03)00035-3 [PubMed: 12591217]

Witter MP, Naber PA, van Haeften T, Machielsen WC, Rombouts SA, Barkhof F, … Lopes da Silva FH (2000). Corticohippocampal communication by way of parallel parahippocampal-subicular pathways. Hippocampus, 10(4), 398–410. 10.1002/1098-1063(2000)10:4<398::AID-HIPO6>3.0.CO;2-K [PubMed: 10985279]

Witter MP, Van Hoesen GW, & Amaral DG (1989). Topographical organization of the entorhinal projection to the dentate gyrus of the monkey. The Journal of Neuroscience, 9(1), 216–228. [PubMed: 2913203]

Wittmann MK, Kolling N, Akaishi R, Chau BK, Brown JW, Nelissen N, & Rushworth MF (2016). Predictive decision making driven by multiple time-linked reward representations in the anterior cingulate cortex. Nature Communications, 7, 12327. 10.1038/ncomms12327

Workman CI, Lythe KE, McKie S, Moll J, Gethin JA, Deakin JF, … Zahn R (2016). Subgenual cingulate-amygdala functional disconnection and vulnerability to melancholic depression. Neuropsychopharmacology, 41(8), 2082–2090. 10.1038/npp.2016.8 [PubMed: 26781519]

Yang T, Bavley RL, Fomalont K, Blomstrom KJ, Mitz AR, Turchi J, … Murray EA (2014). Contributions of the hippocampus and entorhinal cortex to rapid visuomotor learning in rhesus monkeys. Hippocampus, 24(9), 1102–1111. 10.1002/hipo.22294 [PubMed: 24753214]

Yang Y, & Wang JZ (2017). From structure to behavior in Basolateral amygdala-hippocampus circuits. Frontiers in Neural Circuits, 11, 86. 10.3389/fncir.2017.00086 [PubMed: 29163066]

Young MP, Scannell JW, O'Neill MA, Hilgetag CC, Burns G, & Blakemore C (1995). Non-metric multidimensional scaling in the analysis of neuroanatomical connection data and the organization of the primate cortical visual system. Philosophical Transactions of the Royal Society of London. Series B, Biological Sciences, 348(1325), 281–308. 10.1098/rstb.1995.0069 [PubMed: 8577827]

Zikopoulos B, Hoistad M, John Y, & Barbas H (2017). Posterior orbitofrontal and anterior cingulate pathways to the amygdala target inhibitory and excitatory systems with opposite functions. The Journal of Neuroscience, 37(20), 5051–5064. 10.1523/JNEUROSCI.3940-16.2017 [PubMed: 28411274]

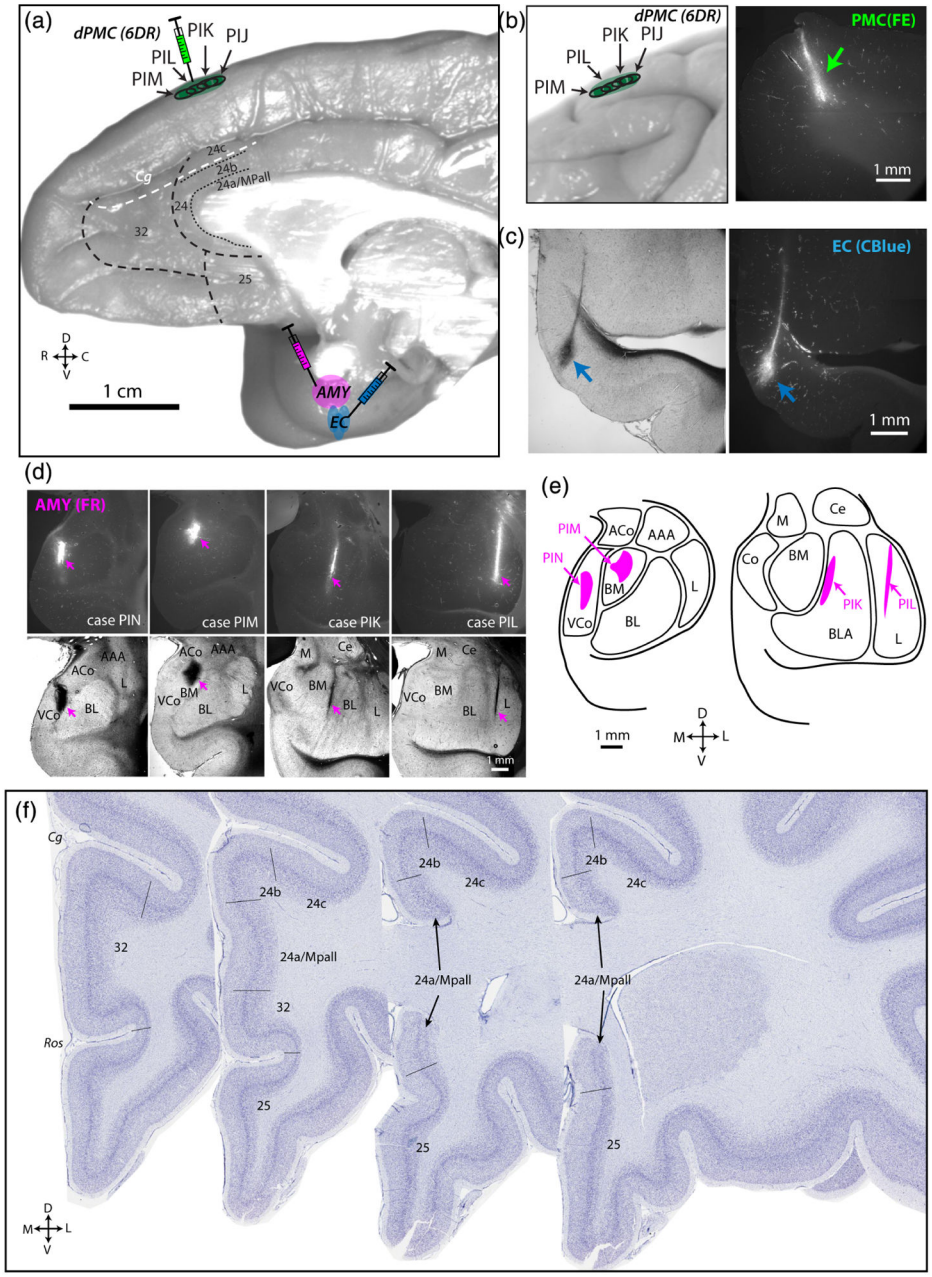

FIGURE 1.

Injection sites and distribution of tracer-labeled connections. (a) Medial view of rhesus monkey brain showing injections in dorsal premotor cortex (PMC), entorhinal cortex (EC), and the amygdala (AMY). (b) Lateral view of rhesus monkey brain and representative fluorescence coronal section photomicrograph showing localization of fluoroemerald (FE) injection sites in dorsal premotor cortical (dPMC). Representative brightfield and fluorescence coronal sections showing injection of cascade blue (CBlue) in anterior EC (c) and fluororuby (FR) tracer in basolateral AMY (d). (e) Coronal section schematic map of AMY injection localization. (f) Photomicrographs of Thionin-stained frontal coronal

sections (http://brainmaps.org) showing boundaries delineating anterior cingulate cortex (ACC) areas, based on previous cytoarchitectonic maps (Barbas & Pandya)

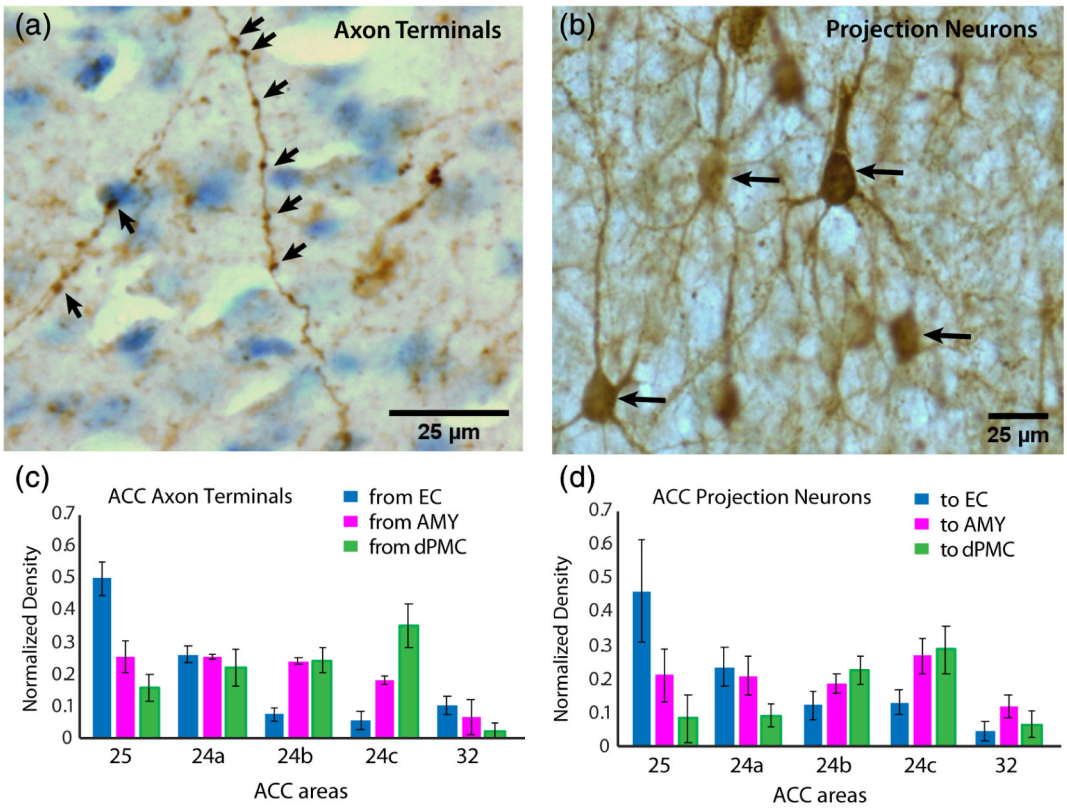

FIGURE 2.

Normalized regional density of anterograde and retrograde tracer label in the anterior cingulate cortex (ACC). (a) High-resolution *z*-projection of a brightfield image stack showing examples of anterograde-labeled axons and axon terminals (arrows). Identified axon terminals appear as boutons or varicosities along visible longitudinally oriented axons within the *z*-stack. (b) *z*-projection of a brightfield image stack showing examples of retrograde-labeled neurons (arrows). (c) Mean normalized regional density of anterograde-labeled axon terminals and (d) retrograde-labeled projection neurons found in distinct ACC areas. Error bars represent *SEM*

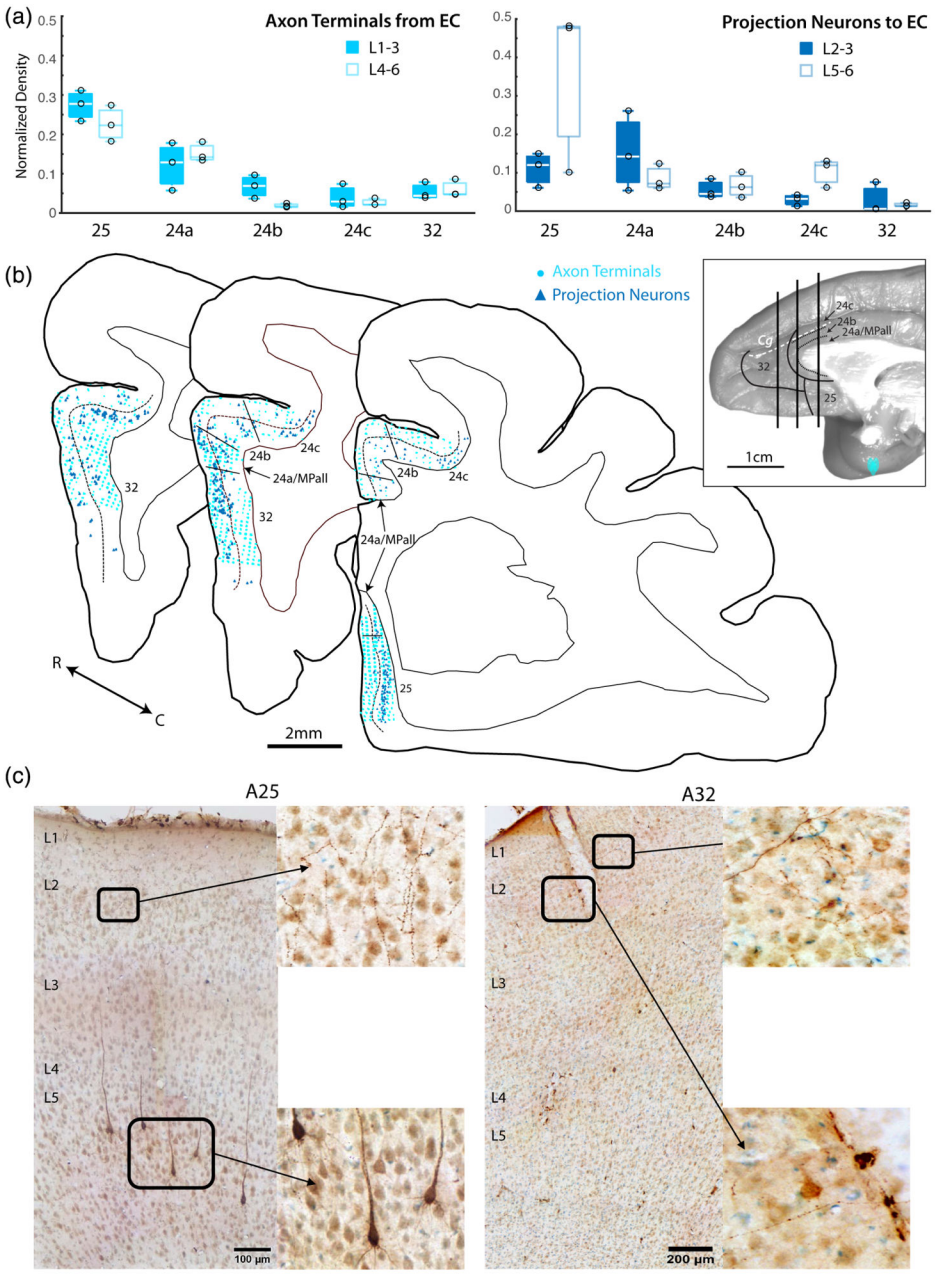

FIGURE 3.

Anterior cingulate cortex (ACC) connections with entorhinal cortex (EC). (a) Box and whisker and vertical scatter plots of normalized laminar density of tracer-labeled axon terminations from EC and projection neurons to EC. (b) Representative coronal maps (case PIN-CBL tracer) of labeled projection neurons and terminations in ACC. Whole brain inset shows location of each slice along the rostro-caudal axis. (c) Representative coronal section photomicrographs of labeled EC projection neurons and terminations in A25 and A32 with Thionin counterstain. Low magnification images show pia to white matter, with laminar labels placed at the top of each layer. Insets are shown in higher magnification

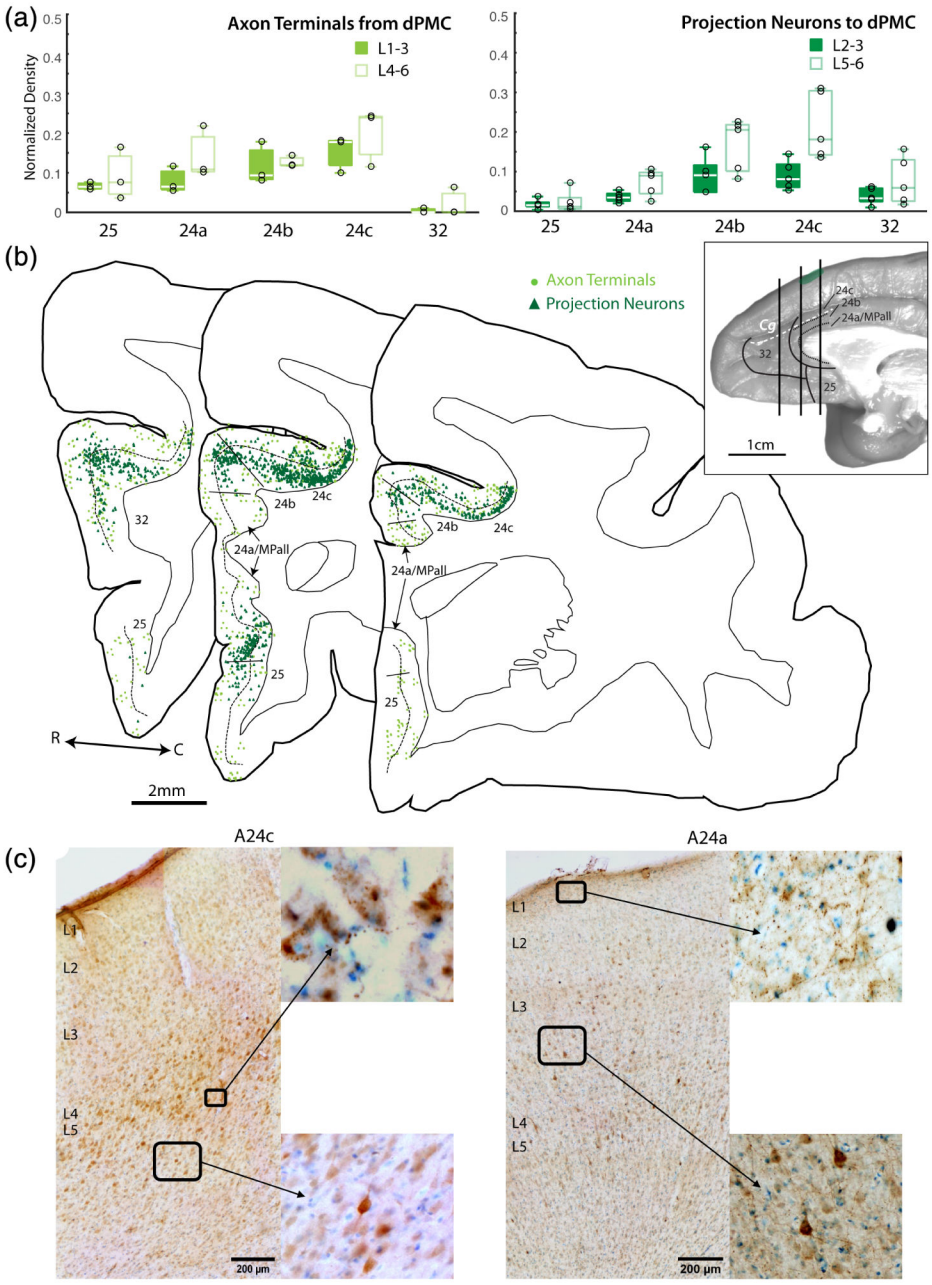

FIGURE 4.

Anterior cingulate cortex (ACC) connections with dorsal premotor cortex (dPMC). (a) Box and whisker and vertical scatter plots of normalized laminar density of tracer-labeled axon terminations from dPMC and projection neurons to dPMC. (b) Representative coronal maps (case PIM-FE tracer) of labeled projection neurons and terminations in ACC. Whole brain inset shows location of each slice along the rostro-caudal axis. (c) Representative coronal section photomicrographs of labeled dPMC projection neurons and terminations in A24c and A24a with Thionin counterstain. Low magnification images show pia to white matter, with laminar labels placed at the top of each layer. Insets are shown in higher magnification

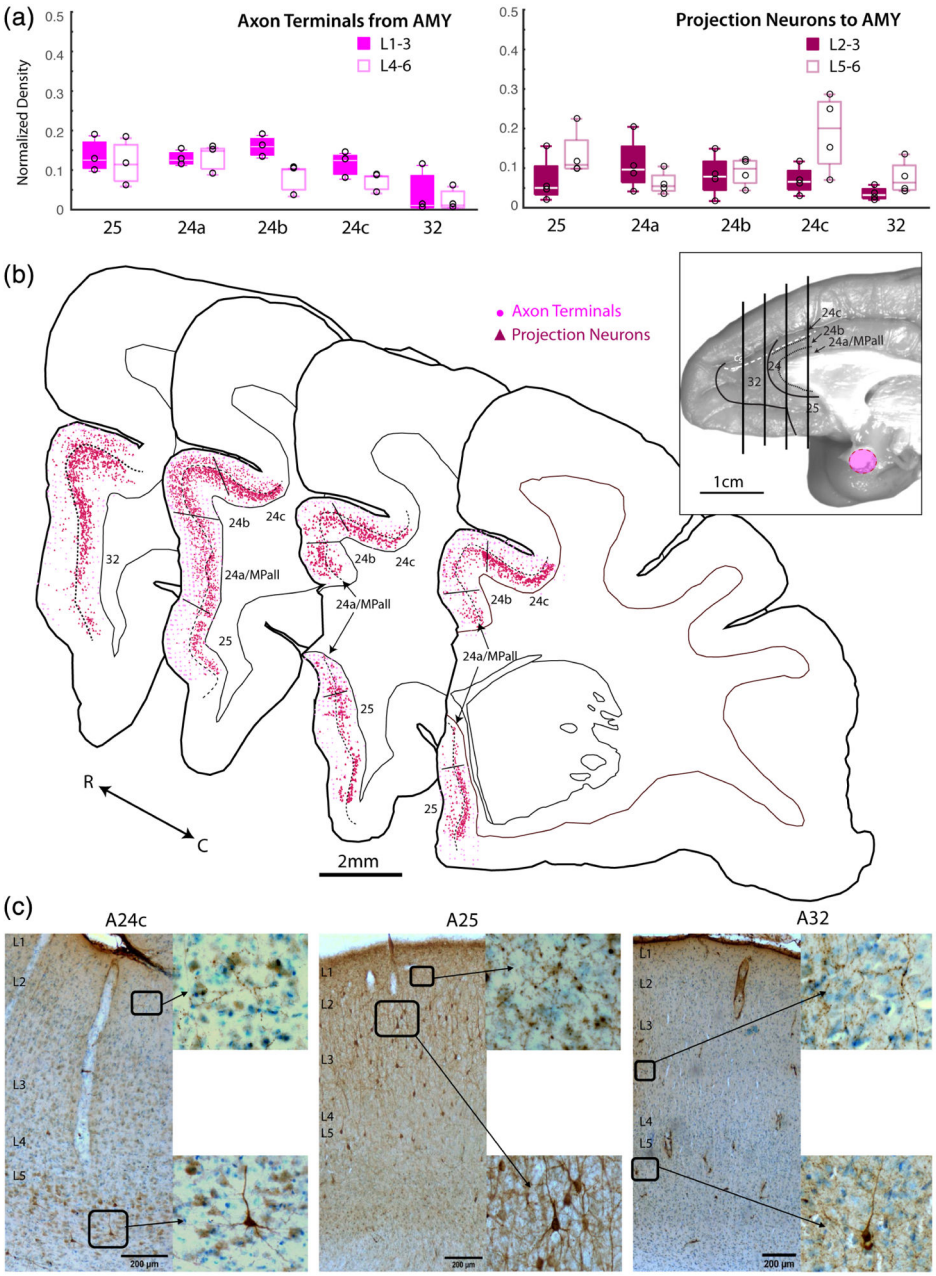

FIGURE 5.

Anterior cingulate cortex (ACC) connections with basolateral amygdala (AMY). (a) Box and whisker and vertical scatter plots of normalized laminar density of tracer-labeled axon terminations from AMY and projection neurons to AMY. (b) Representative coronal maps (case PIM-FR tracer) of labeled projection neurons and terminations in ACC. Whole brain inset shows location of each slice along the rostro-caudal axis. (c) Representative coronal section photomicrographs of labeled AMY projection neurons and terminations in A24c, A25, and A32 with Thionin counterstain. Low magnification images show pia to white matter, with laminar labels placed at the top of each layer. Insets are shown in higher magnification

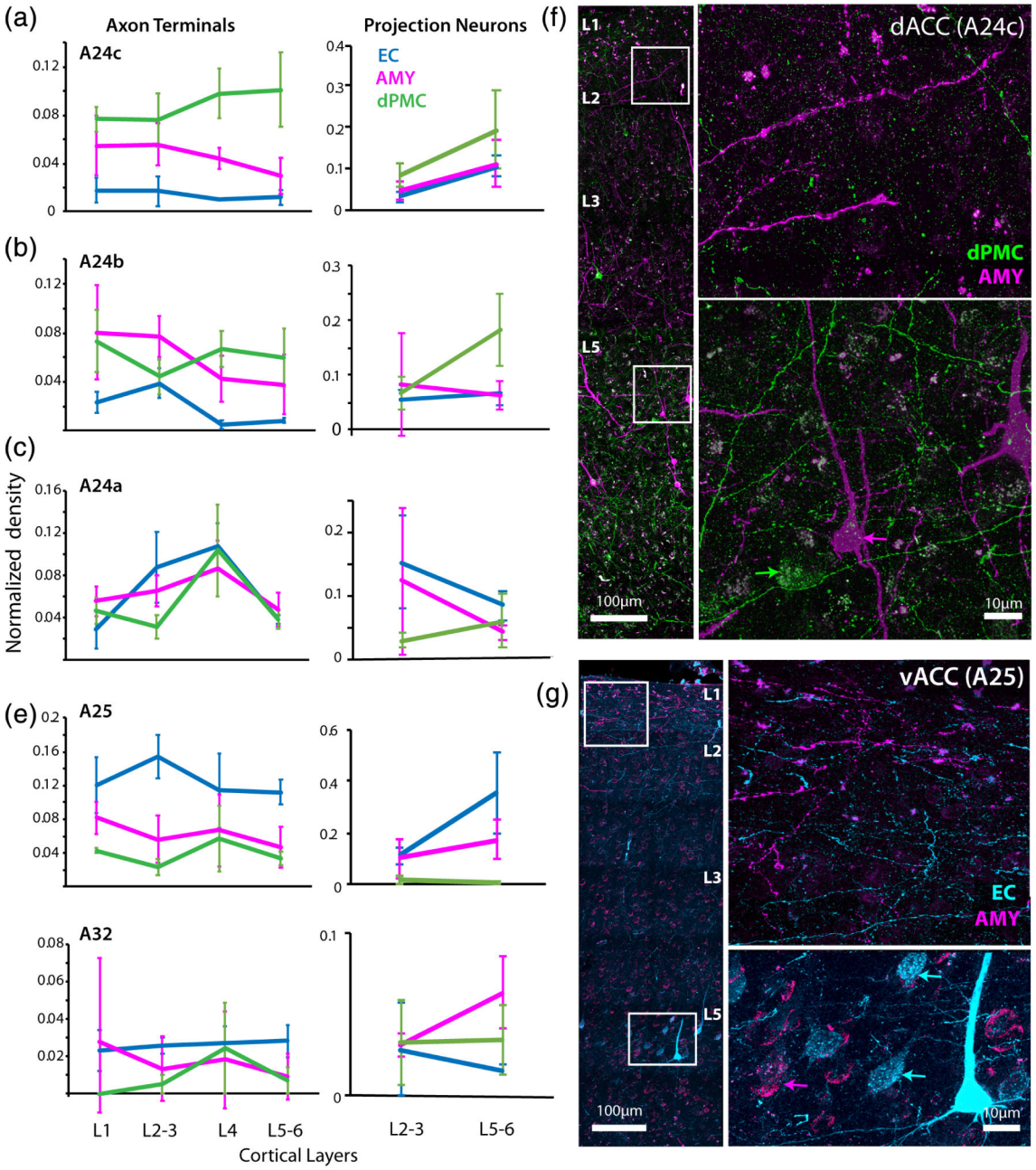

FIGURE 6.

Laminar overlap of entorhinal cortex (EC), dorsal premotor cortical (dPMC), and amygdala (AMY) connections in anterior cingulate cortex (ACC). Mean normalized laminar density of tracer-labeled axon terminations and projection neurons expressed as a proportion of the total label for each tracer in (a) dorsal A24c (MANOVA, Tukey's post-hoc, axon terminals: dPMC vs. AMY $p < .001$; dPMC vs. EC $p < 0.001$; AMY vs. EC $p < 0.01$; projections: dPMC vs. EC $p < .05$), (b) A24b (axon terminals: EC vs. dPMC $p < .05$; EC vs. AMY $p < .05$; projections: dPMC vs. EC $p < .01$), (c) A24a (axon terminals: AMY vs. dPMC $p < .05$; EC vs. dPMC $p < .05$; projections EC vs. dPMC $p < .05$), (d) ventral A25 (axon

terminals: EC vs. AMY $p < .05$; EC vs. dPMC $p < .01$; projections: EC vs. AMY $p < .01$; EC vs. dPMC $p < .05$); (e) A32 (axon terminals and projections: N.S.). Error bars represent *SEM*. (f) Fluorescence confocal stack z-maximum projection image of A24c showing a column of labeled AMY and dPMC connections. Insets in higher magnification show AMY fibers concentrated in the upper layers, and strong overlap of dPMC fibers (green) with dPMC (green arrow) and AMY (magenta arrow) projection neurons in the deep layers (case PIK). (g) Confocal z-maximum projection image of A25 showing overlap of AMY (magenta) and EC (cyan) connections in upper and deep layers. Insets are shown in higher magnification. Labeled AMY and EC fibers are particularly dense in layer 1, and there is strong band of EC fibers in L2–3. In the deep layers, tracer-labeled projection neurons to AMY (magenta arrows) and EC (cyan arrows) are co-mingled

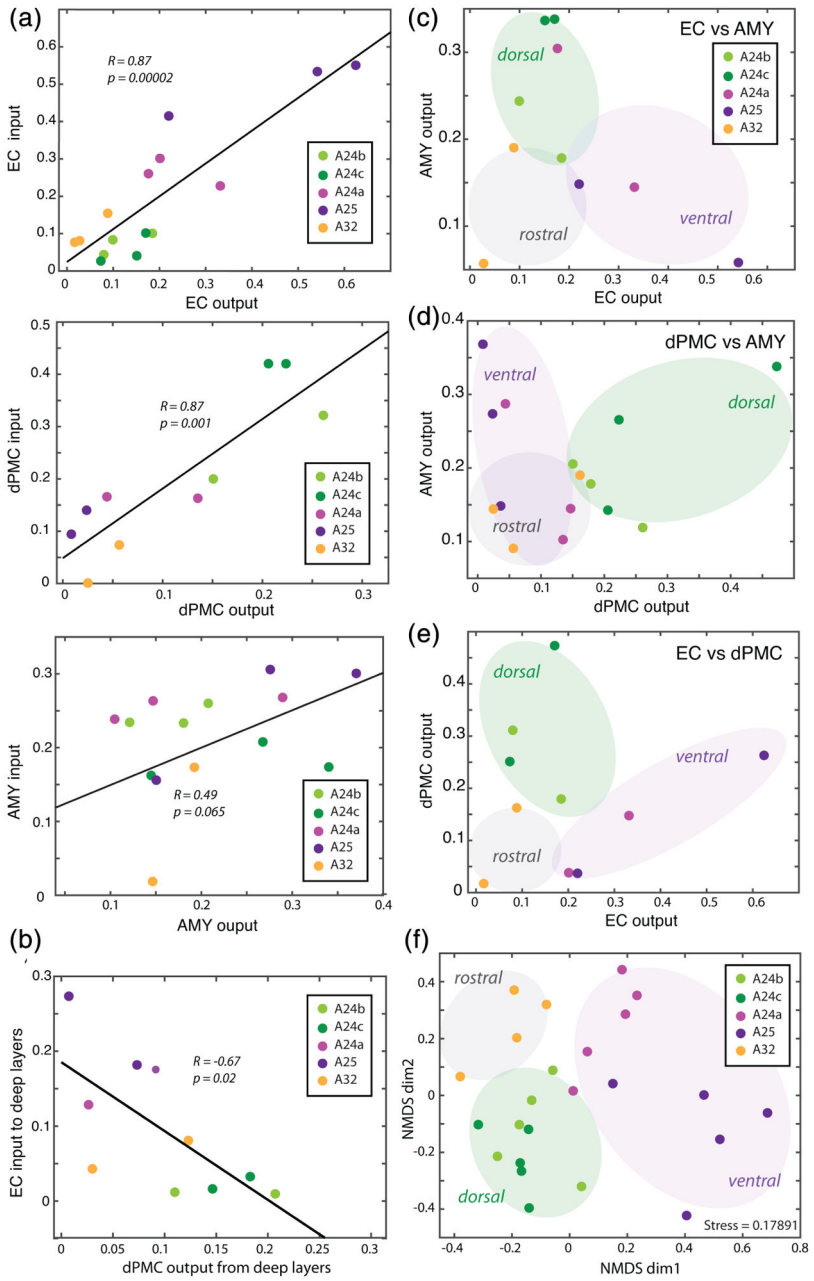

FIGURE 7.

Input–output relationships of entorhinal cortex (EC), dorsal premotor cortical (dPMC), and amygdala (AMY) connections in anterior cingulate cortex (ACC). (a) Scatter plots and linear relationships between the density of tracer-labeled axon terminals (inputs) and projection neurons (outputs) within each pathway. (b) Scatter plot and negative correlation between EC input to deep layers and dPMC output from deep layers. (c–e) Scatter plots of outputs to two injection sites showing clustering of “rostral”, “ventral” and “dorsal” areas based on EC versus AMY outputs (c), dPMC versus AMY outputs (d) and EC versus dPMC outputs (e). (f) Non-metric multidimensional scaling (NMDS) plot showing clustering of areas ACC based on 12 outcome variables as follows: EC, dPMC, and AMY anterograde and retrograde

relative regional densities, percent neurons in L2–3, and percent L4–6 axon terminals in each area. Each point represents an ACC area from each case; the proximity of points indicates the relative similarity based on a distance matrix from pair-wise correlations of multiple variables

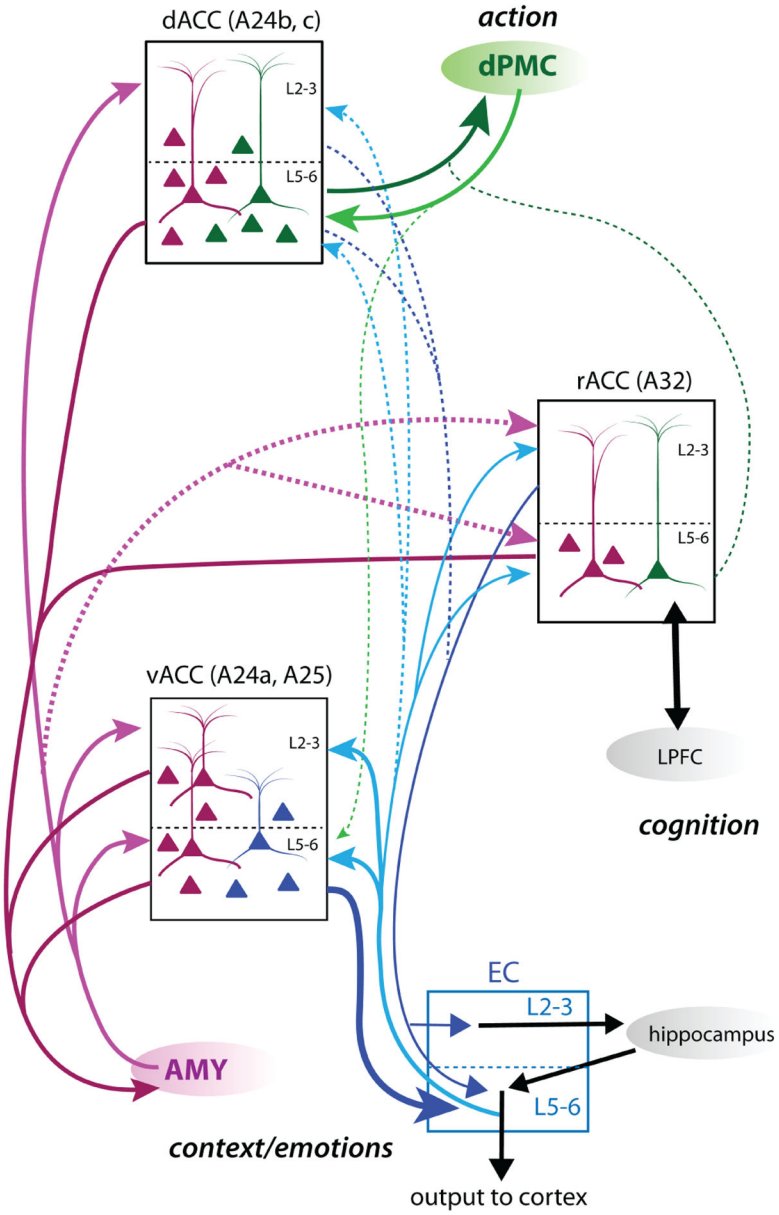

FIGURE 8.

Summary schematic of anterior cingulate cortex (ACC) medial temporal and premotor cortex networks. Schematic showing relative strength and laminar distribution of entorhinal cortex (EC), amygdala (AMY), and dorsal premotor cortical (dPMC) connections in dorsal, ventral, and rostral subdivisions of the ACC. Solid lines represent predominant pathways, and dotted lines represent minor pathways. Line thickness represents the relative strength of connections. dPMC is preferentially connected to the dACC (A24b,c) and EC is preferentially connected to the vACC (A25 and A24a). However, the AMY is strongly distributed across dorsal and ventral ACC areas. vACC thus integrates medial temporal EC and AMY—hippocampal networks for contextual and emotional memory processing. dACC integrates dorsal motor planning with AMY-mediated affective networks. rACC (A32)

integrates moderate AMY and EC connections with moderate-weak dPMC connections. A32 has strong connections with cognitive circuits in lateral prefrontal cortex (LPFC)

TABLE 1

Subjects and injection sites: Summary of the injection sites for each subject showing the total volume injected and the rostro-caudal extent of the core for each injection

		EC injection 3 + 10 kDA (5% sol, 3 μl)		AMY injection 3 + 10 kDA (5% sol, 3 μl)			dPMC injection 3 + 10 kDA (5% sol, 4 μl)	
Case	**Sex, age**	**Tracer analysis**	**R-C extent**	**Tracer analysis**	**R-C extent**	**AMY nucleus**	**Tracer analysis**	**R-C extent**
PIJ	M, 5	FE (bidir.)	0.3 mm	n/a			FR (bidir.)	0.3 mm
PIK	M, 7	n/a		FR (bidir.)	1.2 mm	Basolateral	FE (bidir.)	1.5 mm
PIL	M, 7	n/a		FR (bidir.)	0.3 mm	Lateral	FE (bidir.)	0.6 mm
PIM	F, 6	CBL (bidir.)	0.3 mm	FR (bidir.)	0.6 mm	Basomedial	FE (retro)	0.3 mm
PIN	F, 6	CBL (bidir.)	0.6 mm	FR (retro)	0.6 mm	Cortical	n/a	

Note: Monkeys received injections of bidirectional tracers, fluoroemerald (FE), fluororuby (FR), or Cascade blue (CBL) in the entorhinal cortex (EC), amygdala (AMY), and dorsal pre-motor cortex (dPMC). For all injections a 1:1 cocktail of 10kDA and 3 kDa isotopes for bidirectional tracing was used, with each dye diluted to final concentration of 5% in sterile water. Some cases were used for retrograde (retro) analyses only, or bidirectional (bidir.) analyses of anterograde and retrograde label